NASA
Technical
Paper
3215

March 1992

Time-Frequency Representation of a Highly Nonstationary Signal Via the Modified Wigner Distribution

T. F. Zoladz,
J. H. Jones,
and J. Jong

NASA

NASA Technical Paper 3215

1992

Time-Frequency Representation of a Highly Nonstationary Signal Via the Modified Wigner Distribution

T. F. Zoladz
and J. H. Jones
George C. Marshall Space Flight Center
Marshall Space Flight Center, Alabama

J. Jong
Wyle Laboratories
Huntsville, Alabama

NASA
National Aeronautics and Space Administration
Office of Management
Scientific and Technical Information Program

TABLE OF CONTENTS

TECHNICAL PAPER

TIME-FREQUENCY REPRESENTATION OF A HIGHLY NONSTATIONARY SIGNAL VIA THE MODIFIED WIGNER DISTRIBUTION

I. INTRODUCTION

This report describes and evaluates a new signal processing technique called the modified Wigner distribution (MWD) used for the spectral analysis of highly nonstationary multicomponent signals. The regular Wigner distribution (WD) is capable of providing high resolution time-frequency estimates of nonstationary signals which are common in many fields including the dynamic response of rotating machinery. A traditional tool for such analysis has been the short-time Fourier transform (STFT), commonly referred to as "overlap" processing, which is obtained by applying a fixed-length moving time window to nonstationary data prior to performing the fast Fourier transform (FFT). However, if spectral components within the signal vary considerably in frequency during the time window, the STFT often fails in providing enough frequency resolution to identify key time-frequency spectral characteristics.

The WD was originally introduced in 1932 by E. Wigner.[1] It received little attention until 1980 when Claasen and Mecklenbrauker[2] presented a comprehensive three-part paper describing the utility of the WD as a tool for time-frequency analysis of nonstationary signals.

Major obstacles arise in the direct use of the WD. Most notable of these problems are aliasing and the generation of artifacts or "phantom" spectral peaks in the resultant time-frequency distribution. A number of attempts, with varying degrees of success, have been employed to minimize these effects.[3–5] This paper presents yet another approach. With the introduction of the "smart window," this approach will hopefully overcome these obstacles.

The MWD will have important application in turbomachinery diagnostic analysis. It is particularly suited to those turbomachinery operations which are highly transient, i.e. during startup or ramping conditions. It can also be an important diagnostic tool in failure analysis where the dynamic signals are highly nonstationary.

II. THE WIGNER DISTRIBUTION

The WD is a powerful tool in determining the time-frequency characteristics of a highly nonstationary signal. The technique has been applied successfully in the identification of abnormal machine operating states through vibration signal analysis.[3] Other applications of the WD include the analysis of time-varying spectra in optics, speech, sonar, and seismic signal processing.

The WD of a real signal $r(t)$ is given by:

$$W(t,f) = \int z(t+\tau/2)\, z^*(t-\tau/2)\, e^{j2\pi f\tau}\, d\tau \ , \qquad (1)$$

where $z(t)$ is the analytic signal of $r(t)$, $z(t) = r(t) + j\, i(t)$, and $i(t)$ is the Hilbert transform (HT) of $r(t)$, $i(t) = \mathrm{HT}\{r(t)\}$. Let the absence of limits on the integral symbol denote the interval $(-\infty, \infty)$. In equation (1), $z^*(t)$ represents the complex conjugate of the analytic signal $z(t)$. Therefore, the WD is the Fourier transform (FT) of the product between the original forward signal and corresponding backward signal both centered at time t. If the frequency of a subject narrowband signal is either monotonically increasing or decreasing within its time window, the product of this forward and backward signal will provide frequency cancellation, and, as a result, will estimate a frequency corresponding to the signal frequency at the center of the time window. However, the product in equation (1), which serves as the kernel of the FT, introduces a frequency summing effect. Taking a real single component signal with a discrete component at f_o as an example, the summing effect produces a peak in the WD spectrum at $2f_o$. For this reason, equation (1) scales the subject time signal by two. However, this scaling is only aesthetic and does not relax sampling constraints on the time signal. If $2f_o$ is greater than the original Nyquist frequency (determined when the subject time signal was originally sampled) aliasing within the WD spectrum will occur. For this reason, an analytic signal is used in equation (1) since it has no energy at negative frequencies. Aliasing due to the frequency summing effect can now be avoided, and, in addition, frequency difference effects (coupling between positive and negative frequency components) are eliminated. Essentially, use of the analytic signal in equation (1) returns the sampling rate constraint for a subject time signal back to its original Nyquist rate.

Prior to introducing the MWD, sample graphical illustrations of the WD for cases involving simple sinusoids will be presented. In the examples, the WD's will be processed through convolution in the frequency domain since this format conveys the frequency summing and difference effects well.

Before developing case I of the WD, equation (1) will be simplified into a convenient form representing convolution in the frequency domain. Taking the original equation and replacing $\tau/2$ with τ, gives

$$W(t,f) = \int z(t+\tau)\, z^*(t-\tau)\, e^{j2\pi f\tau}\, d\tau \ . \tag{2}$$

Note, with removal of $\tau/2$ from the WD equation, f now represents twice the actual frequency of spectral components contained in the original time signal. To simplify further evaluation, one should just consider one cross section of the WD at $t = t_o$

$$W(t_o,f) = \int z(t_o+\tau)\, z^*(t_o-\tau)\, e^{j2\pi f\tau}\, d\tau \ . \tag{3}$$

Letting

$$x(t) \equiv z(t_o+\tau)$$

$$y(t) \equiv z^*(t_o-\tau) \ .$$

Equation (3) can be viewed as the FT of the product $x(t)y(t)$

$$W(t_o,f) = FT\{x(t)y(t)\} \ . \tag{4}$$

The FT of the product $x(t)y(t)$ can also be viewed as a convolution in the frequency domain. Given that

$$x(t) \Leftrightarrow X(\alpha)$$

$$y(t) \Leftrightarrow Y(\alpha)$$

where $\Leftrightarrow$ denotes FT pair.

Equation (4) can now be written as the convolution

$$W(t_o,f) = \int X(\alpha)Y(f-\alpha)\, d\alpha \ . \tag{5}$$

This form of the WD will be used in the following graphical evaluations.

WD CASE I: ANALYTIC SIGNAL CONTAINING SINGLE SINUSOID

For this case, the real signal is a single sinusoid at frequency f_o

$$r(t) = \cos(2\pi f_o t) \ .$$

The imaginary portion of the analytic signal, $z(t)$, is calculated through the HT of the real signal

$$i(t) = \mathrm{HT}\{\cos(2\pi f_o t)\} = \sin(2\pi f_o t) \ .$$

The analytic signal, $z(t)$, now becomes

$$z(t) = \cos(2\pi f_o t) + j \sin(2\pi f_o t) = e^{j\,2\pi f_o t} \ .$$

The complex conjugate of $z(t)$ is

$$z^*(t) = e^{-j2\pi f_o t}$$

and

$$z^*(-t) = e^{j2\pi f_o t}$$

Moreover, the FT of both $z(t)$ and $z^*(-t)$ is a delta function shifted by f_o.

$$\mathrm{FT}\{e^{j2\pi f_o t}\} = \delta(f-f_o)$$

This sample case is now in proper form with respect to equation (4), with

$$x(t) = z(\tau) \ ,$$

$$y(t) = z^*(-\tau) \ , \qquad (t_o = 0)$$

and

$$X(f) = \delta(f-f_o) \ ,$$

$$Y(f) = \delta(f-f_o) \ .$$

With $t_o = 0$, equation (5) can be written as a function of frequency only

$$W(f) = \int X(\alpha)\, Y(f-\alpha)\, d\alpha \ , \qquad (6)$$

and the WD for case I can now be developed graphically (fig. 1) through convolution in the frequency domain.

The left-hand side of figure 1 displays the translation of the $Y(-\alpha)$ spectrum during the convolution process defined by equation (6). The right-hand side of the figure shows successive contributions to the WD spectrum as the frequency, f, varies during the convolution. For this case involving the analytic signal of a single sinusoid, a contribution to $W(f)$ is made only when $f = 2f_o$. Remembering that f now represents twice the actual frequency of spectral components contained in the original time signal, f must be scaled by $1/2$ to yield a correct frequency value. In this case, the true frequency would be $2f_o/2$, or f_o, which is the expected result.

WD CASE II: ANALYTIC SIGNAL CONTAINING MULTIPLE SINUSOIDS

For this case, the real signal is composed of two sinusoids at frequencies of f_1 and f_2

$$r(t) = \{\cos(2\pi f_1 t) + \cos(2\pi f_2 t)\}$$

This case is identical to WD case I except that the real signal contains two discrete components. Using the same method of reduction as in the previous case yields

$$X(f) = \delta(f-f_1)+\delta(f-f_2) \ ,$$

$$Y(f) = \delta(f-f_1)+\delta(f-f_2) \ .$$

Again, using equation (6), the WD for case II can be developed graphically (fig. 2) through convolution in the frequency domain.

As in figure 1, the left-hand side of figure 2 displays the translation of the $Y(-\alpha)$ spectrum during the convolution defined by equation (6), and, the right-hand side shows successive contributions to the WD spectrum as the frequency, f, varies. Since the original time signal contains multiple discrete components, peaks in the WD spectrum are generated when $f = 2f_1$ and $f = 2f_2$. Again, scaling by $1/2$ yields the correct frequency representations of the spectral components. However, in this case, the WD spectrum also exhibits a contribution at $f = f_1+f_2$. This contribution is due to cross term coupling between the components at f_1 and f_2. This coupling is displayed in figure 2 where the peaks b and c of the $X(\alpha)$ spectrum line up with peaks c and b of the $Y([f_1+f_2] - \alpha)$ spectrum. This cross coupling effect contributes a peak to the WD spectrum at the frequency $[f_1+f_2]$. After scaling, this false peak would appear in the WD spectrum at a frequency of $[f_1+f_2]/2$.

Generation of false peaks due to cross coupling effects severely limits the practical application of the WD since few real world signals are single component. As shown in the previous

example, use of the conventional WD in developing time-frequency representations of multi-component signals, even with the use of an analytic signal, introduces erroneous spectral components. These "phantom" peaks only confuse the resulting WD spectrum.

III. THE MODIFIED WIGNER DISTRIBUTION

In order for the WD to perform as a practical tool in the time-frequency analysis of multi-component signals, unwanted erroneous spectral components due to cross coupling among both negative, and most notably, positive frequency components in these signals must be eliminated. The MWD accomplishes this. Thus, the superior time-frequency resolution of the WD can be attained without the generation of "phantom" spectral peaks.

For a cross section of the time-frequency representation of a real signal $r(t)$, at $t = t_o$, the MWD is introduced and is defined by:

$$M(t_o,f) = \int \mathbb{W}(\alpha - f/2)\, X(\alpha)\, Y(f-\alpha)\, d\alpha \quad , \tag{7}$$

where

$$x(t) \equiv r(t_o+t) \quad ,$$

$$y(t) \equiv r(t_o - t) \quad ,$$

and

$$X(f) \Leftrightarrow x(t) \quad ,$$

$$Y(f) \Leftrightarrow y(t) \quad .$$

As equation (7) suggests, the MWD is evaluated in the frequency domain using the FT's of a real time signal centered at t_o and its respective reversed signal also centered at t_o.The central trait of the MWD which separates the new technique from the traditional WD is its smart frequency window function, $\mathbb{W}(f)$. Use of this window function eliminates the cross coupling of positive frequency components. This in turn prevents erroneous spectral peaks from entering the MWD time-frequency representation during the evaluation of a multicomponent signal. Moreover, use of the smart window, $\mathbb{W}(f)$, eliminates cross coupling between positive and negative frequency components by preventing their interaction during the evaluation of the MWD. There are some limitations on the use of the smart window, and they will be discussed later. The MWD does not rely on the use of the analytic signal of the subject time signal; thus, the HT of the original time signal is no longer necessary. Finally, since the MWD is evaluated in the frequency domain, aliasing due to the frequency summing effect is avoided.

As with the WD, the evaluation of the MWD will also be illustrated graphically. Where the WD was reduced to a more convenient form representing convolution in the frequency domain to simplify its graphical presentation, the MWD is actually evaluated through convolution in the frequency domain. The graphical evaluations of MWD's which follow include the same two cases which were presented for the WD. MWD case I develops the spectrum for a real signal containing a single sinusoid while MWD case II evaluates a real signal containing multiple sinusoids.

Using equation (7), MWD cases I and II can be developed graphically through convolution in the frequency domain.

MWD CASE I: REAL SIGNAL CONTAINING SINGLE SINUSOID

The real signal to be evaluated is a single sinusoid at frequency f_o

$$r(t) = \cos(2\pi f_o t) \ .$$

The required time signals centered at t_o are

$$x(t) = \cos\{2\pi f_o(t_o+t)\} \ ,$$

$$y(t) = \cos\{2\pi f_o(t_o-t)\} \ .$$

To simplify the evaluation, let $t_o = 0$, yielding

$$x(t) = \cos\{2\pi f_o(+t)\} \ ,$$

$$y(t) = \cos\{2\pi f_o(-t)\} \ .$$

Fourier transformation of $x(t)$ and $y(t)$ gives $X(f)$ and $Y(f)$

$$X(f) = \delta(f-f_o)+\delta(f+f_o) \ ,$$

$$Y(f) = \delta(f+f_o)+\delta(f-f_o) \ .$$

$X(f)$ and $Y(f)$ are equivalent with both frequency representations consisting of two delta functions, one delta function being shifted along the positive frequency axis by f_o and the other shifted along the negative frequency axis by f_o. Using equation (7), the MWD for case I can be developed graphically (fig. 3).

Figure 3 is essentially the same as figure 1 which displays the development of the WD for a signal containing a single discrete component. However, since the MWD operates on real signals, the $X(\alpha)$ and $Y(\alpha)$ spectra also contain negative frequency components. Moreover, figure 3 introduces the smart window function, $\mathbb{W}(f)$. The window function is a gate in the frequency domain of unity amplitude which translates along the dummy variable (α) axis at one half the rate of the $Y(-\alpha)$ spectrum translation during the convolution. The window, as shown in figure 3, has a width in frequency of 2m. This width parameter is almost inconsequential in the processing of single component signals such as in this case, but a proper window width is very critical in the evaluation of multicomponent signals. As previously stated, the window, $\mathbb{W}(f)$, eliminates cross coupling between positive and negative frequency components by preventing their interaction. Moreover, it eliminates interaction between components in a multicomponent signal. The window function's influence on a multicomponent signal will be discussed in MWD case II. For a single component signal, unwanted cross coupling would have contributed a false spectral peak at zero frequency; however, the gating action provided by the window function prohibits this coupling.

For this case involving a real signal containing a single sinusoid, a contribution to the MWD spectrum, $M(f)$, is made only when $f = 2f_o$. Notice, that when the $Y(-\alpha)$ spectrum has translated

along the α axis by $2f_o$, the window function, $\mathbf{W}(f)$ has translated by a frequency of one half of $2f_o$, or, f_o. This positioning of the window function permits the desired coupling which only provides a contribution to the MWD spectrum at $f = 2f_o$. Again, this f must be scaled by $1/2$ to yield a correct frequency value. This yields the expected frequency of f_o.

MWD CASE II: REAL SIGNAL CONTAINING MULTIPLE SINUSOIDS

In this case, the real signal consists of two sinusoids at frequencies of f_1 and f_2

$$r(t) = \{\cos(2\pi f_1 t) + \cos(2\pi f_2 t)\} \ .$$

This case is identical to MWD case I except that the real signal now contains two discrete components. Similar simplification as in the previous case yields the frequency representations of the time signals $x(t)$ and $y(t)$ with

$$X(f) = \delta(f-f_2) + \delta(f-f_1) + \delta(f+f_1) + \delta(f+f_2) \ ,$$

$$Y(f) = \delta(f+f_2) + \delta(f+f_1) + \delta(f-f_1) + \delta(f-f_2) \ .$$

With these frequency representations, the MWD for case II can be developed graphically (fig. 4) using equation (7).

As in the previous example, figure 4 shows how the positioning of the window function allows desired couplings which in turn make correct contributions to $M(f)$. These couplings result in peaks at the frequencies $2f_1$ and $2f_2$ in the final MWD spectrum. However, the key feature of the MWD, which separates it from the conventional WD, is its ability to eliminate the cross coupling of positive frequency components. This is shown in figure 4 when f = f_1+f_2. At this value of f, notice that the components b and c of the $X(\alpha)$ spectrum line up with peaks c and b, respectively, of the $Y([f_1+f_2]-\alpha)$ spectrum. This is a graphic representation of cross coupling between positive frequency components. This cross coupling is eliminated by the positioning of the frequency window. Notice how the smart window is positioned between the components c and b in the $Y([f_1+f_2]-\alpha)$ spectrum thereby preventing cross coupling. In this situation, the width of the frequency window is critical since too wide a window would permit cross coupling. For this reason, the frequency resolution of the MWD in differentiating spectral peaks is governed by the window function, $\mathbf{W}(f)$. In figure 4, if $[f_2-f_1]$ were less than the window width, 2m, cross coupling between positive frequency components would occur and erroneous peaks would be contributed to the MWD spectrum just as in WD case II.

IV. IMPLEMENTATION OF THE MODIFIED WIGNER DISTRIBUTION IN DIGITAL FORMAT

Before developing a digital representation of the MWD, its general form given by equation (7) will be simplified. Starting with equation (7)

$$M(t_o,f) = \int \mathbf{W}(\alpha-f/2)\, X(\alpha)\, Y(f-\alpha)\, d\alpha \ , \qquad (7)$$

where

$$x(t) \equiv r(t_o+t) \ ,$$

$$y(t) \equiv r(t_o-t) \ ,$$

and

$$X(f) \Leftrightarrow x(t) \ ,$$

$$Y(f) \Leftrightarrow y(t) \ .$$

Again, equation (7) defines a cross section of $M(t,f)$ at $t = t_o$. By defining

$$\beta = (f/2) - \alpha \ ,$$

equation (7) becomes

$$M(t_o,f) = -\int \mathbf{W}(-\beta)\, X([f/2] - \beta)\, Y([f/2] + \beta)\, d\beta \ . \tag{8}$$

Letting $f' = (f/2)$ yields

$$M(t_o,f') = -\int \mathbf{W}(-\beta)\, X(f'-\beta)\, Y(f'+\beta)\, d\beta \ . \tag{9}$$

Since the window function is symmetric, $\mathbf{W}(-\beta) = \mathbf{W}(\beta)$ and equation (9) becomes

$$M(t_o,f') = -\int \mathbf{W}(\beta)\, X(f'-\beta)\, Y(f'+\beta)\, d\beta \ . \tag{10}$$

Finally, by letting $\gamma = -\beta$, and by invoking symmetry of the frequency window once again, the MWD representation becomes

$$M(t_o,f') = \int \mathbf{W}(\gamma)\, X(f'+\gamma)\, Y(f'-\gamma)\, d\gamma \ . \tag{11}$$

Note, that in this form, the MWD represents a frequency which no longer needs scaling. Moreover, equation (11) is in a form conducive to digital implementation. The digital form of equation (11) is

$$M(k) = \sum_{i=-m}^{+m} X(k+i)\, Y(k-i) \ , \tag{12}$$

where $X(k)$ is the discrete Fourier transform (DFT) of a subject real time series, $x(n)$, centered at t_o, and $Y(k)$ is the DFT of $y(n)$, the reversal of $x(n)$, also centered at t_o. $M(k)$ represents the discrete MWD spectrum of a time signal centered at t_o, and the summation limits in equation (12) constitute the smart window function. Since $y(n)$ is the reversal of $x(n)$, it can easily be proven that,

$$Y(k) = X^*(k)\, W_N^{-k} \ . \tag{13}$$

where

$$W_N \equiv e^{-j(2\pi/N)} \ .$$

N denotes the number of discrete values in the time history used in calculation of the spectrum with n serving as a position index. Finally, by combining equation (13) and (12), the final form of the digital representation of the MWD is attained

$$M(k) = \sum_{i=-m}^{+m} X(k+i)\, X^*(k-i)\, W_N^{-(k-i)} \quad . \tag{14}$$

Equation (14) states that the evaluation of the MWD at frequency k is simply the sum of the left-hand side and right-hand side of a signal's FFT spectrum, $X(k)$, with both sides centered at frequency k, modified by a phase correction term of unity amplitude. Note, that when no window is applied ($m = 0$), the MWD reduces to a special form with an amplitude equal to the power spectral density (PSD) but modified by a phase term.

V. WIGNER AND MODIFIED WIGNER DISTRIBUTION EXAMPLES

In order to test the capability of the MWD in extreme situations, a simulated sine wave varying linearly in frequency at a rate of ~400,000 Hz/s was processed using both the traditional STFT method and the MWD. Figure 5 shows the STFT isoplot (logarithmic in amplitude) of a sine wave whose frequency first decreases then increases rapidly at this rate within 25 ms. The sampling frequency in this case is 10,240 Hz, and the length of the moving time window is 12.5 ms (corresponding to 128 discrete data points) with 20 Hanning windows applied. Use of the Hanning window makes the effective time window approximately 3 ms. As seen in figure 5, the STFT produces a very broad spectral peak since the frequency of the component varies considerably during each window. However, figure 6 shows the superior frequency resolution gained by the MWD (equation (14)) in processing the same simulated signal. Figure 7 shows the block of raw time data used in determining the first spectrum of the isoplots in figures 5 and 6. Along with this raw time signal, figure 7 also identifies the actual input simulated frequency at time 0.00625 s, the center of the first block of data. This frequency, 2,550 Hz, will serve as the benchmark in comparing the accuracy of the spectra generated by the STFT and MWD. Figure 8 shows the first spectra of figures 5 and 6 in linear format. The increased frequency resolution attained by the MWD is readily apparent. Moreover, the MWD is much more accurate in estimating the actual signal frequency at the center of the time window. While the STFT overestimated this frequency by 110 Hz, the MWD estimation was within 40 Hz. Again, this increased accuracy can be attributed to the frequency cancellation effect inherent to the MWD. Notice in figure 6 that, during the turn in frequency of the single component signal, lobing on the inside turn of the time-frequency representation becomes prominent since the frequency cancellation effect inherent to the MWD is limited during this extreme transitional period in which the signal is neither monotonically increasing or decreasing.

The isoplot of figure 9 has been developed through the STFT of a simulated sine wave whose frequency and amplitude both varied rapidly within the 400 ms of activity displayed. The length of the moving time window in the STFT is 25 ms with a sampling frequency of 10,240 Hz. Within the span of each time window, the frequency of the simulated sine wave changes approximately 300 Hz. For this reason, STFT of the signal produces a very broad spectral peak. Figure 10 shows the conventional WD spectrum for the same signal processed using the same parameters as the STFT. The increased frequency resolution relative to figure 9 is very evident. Figure 11 shows the corresponding MWD spectrum for the signal, which, in this case, provides just as much frequency resolution as the WD.

As shown in the previous figures, relative to traditional techniques, both the WD and MWD provide increased frequency resolution for a single component signal. However, this is not the case in the evaluation of multiple components signals. Figure 12 shows the STFT isoplot of a simulated

signal composed of two sine waves. As before, the frequencies and amplitudes of the discrete components are changing rapidly, and the corresponding spectral peaks are very broad. The WD spectrum for the same signal processed using the same parameters is shown in figure 13. With the multicomponent signal, the analysis form of the WD introduces an erroneous cross coupling component between the two simulated sine waves. This "phantom" peak train confuses the resulting time-frequency representation of the multiple component signal. Figure 14 is the corresponding MWD spectrum for the multicomponent signal. As can be seen in the figure, a high frequency resolution is attained (much improved over that of the STFT method) without unwanted cross coupling terms corrupting the time-frequency representation.

Figure 15 is a PSD isoplot showing the shutdown of an SSME alternate turbopump development (ATD) test rig following a component failure. As seen in the STFT isoplot, following the failure which occurs at 615 s into the test, the spectral distribution of the proximity probe signal becomes very noisy. In order to study the temporal and spectral characteristics of the signal just prior and following the failure, analysis focused on a very short time period around 615 s. Figure 16 shows the STFT isoplot for a 300-ms period extending from 615 to 615.3 s. No clear spectral characteristics can be identified in this time-frequency representation of the proximity probe measurement. Figure 17 is the MWD spectrum for the same period using identical processing parameters. While use of the traditional WD would introduce numerous erroneous spectral components in trying to improve upon the performance of the STFT, the MWD is successful in providing a much clearer time-frequency picture of the time signal without the "phantom" peaks.

As a final example, figure 18 is an "overlapped" (STFT) isoplot developed during the failure investigation of space shuttle main engine u/n 0215. During test 901-666, the engine experienced a premature cutoff due to a second-stage turbine-blade failure in the high pressure fuel turbopump (HPFTP) u/n 5602R1. The 0–1-kHz isoplot of figure 18 displays the time-frequency history of the fundamental shaft rotational (synchronous) frequency, N, as taken from an external pump-end accelerometer. As evidenced by the sudden increase in synchronous amplitude in the figure, the pump failure initiated at approximately 3.9 s into the test. The STFT and MWD isoplots for the pump speed transducer channel are shown in figure 19. The speed probe is a magnetic-type transducer which registers four "blips" with every revolution of the pump shaft, and, for this reason, the $4N$ component dominates both isoplots. Note the increased frequency resolution offered in the MWD plot of figure 19, especially during the ramp-down period following the failure. In order to attain more insight regarding the failure, attention was focused on the 100 ms timeframe surrounding the failure. Figure 20 shows the STFT and MWD isoplots for this extremely short period. Again, notice the increased frequency resolution offered by the MWD. Moreover, note the enhancement of the novel character of the frequency variation. The frequency separation exhibited in both plots at N, $2N$, $3N$, and $5N$ is currently interpreted as being caused by a phase discontinuity in these respective frequency components of the speed signal at the time of the failure. This phase discontinuity of the shaft precession can be attributed to the sudden turbine blade loss which instantaneously shifted the phase of the driving imbalance force. The frequency branching effect does not appear in the $4N$ component (which represents the pure shaft rotational motion, or motion other than precession) since the speed probe continues to count four "blips" per revolution regardless of the phase discontinuity at the time of the failure. It is also important to note that as a result of the branching (forking) of the frequencies, an artifact is present in the middle of the fork. This results because the difference between the upper and lower frequencies of the branch is within the bandwidth of the smart window.

VI. CONCLUDING REMARKS

The modified Wigner distribution has proven very successful in determining time-frequency representations of highly nonstationary multicomponent signals. The MWD offers the same time-frequency resolution as the traditional Wigner distribution; however, through use of a "smart" frequency window, it eliminates the annoying cross coupling artifacts inherent to the WD. This ability to eliminate "phantom" spectral components along with its simplistic implementation make the modified Wigner distribution a promising real-world signal analysis tool.

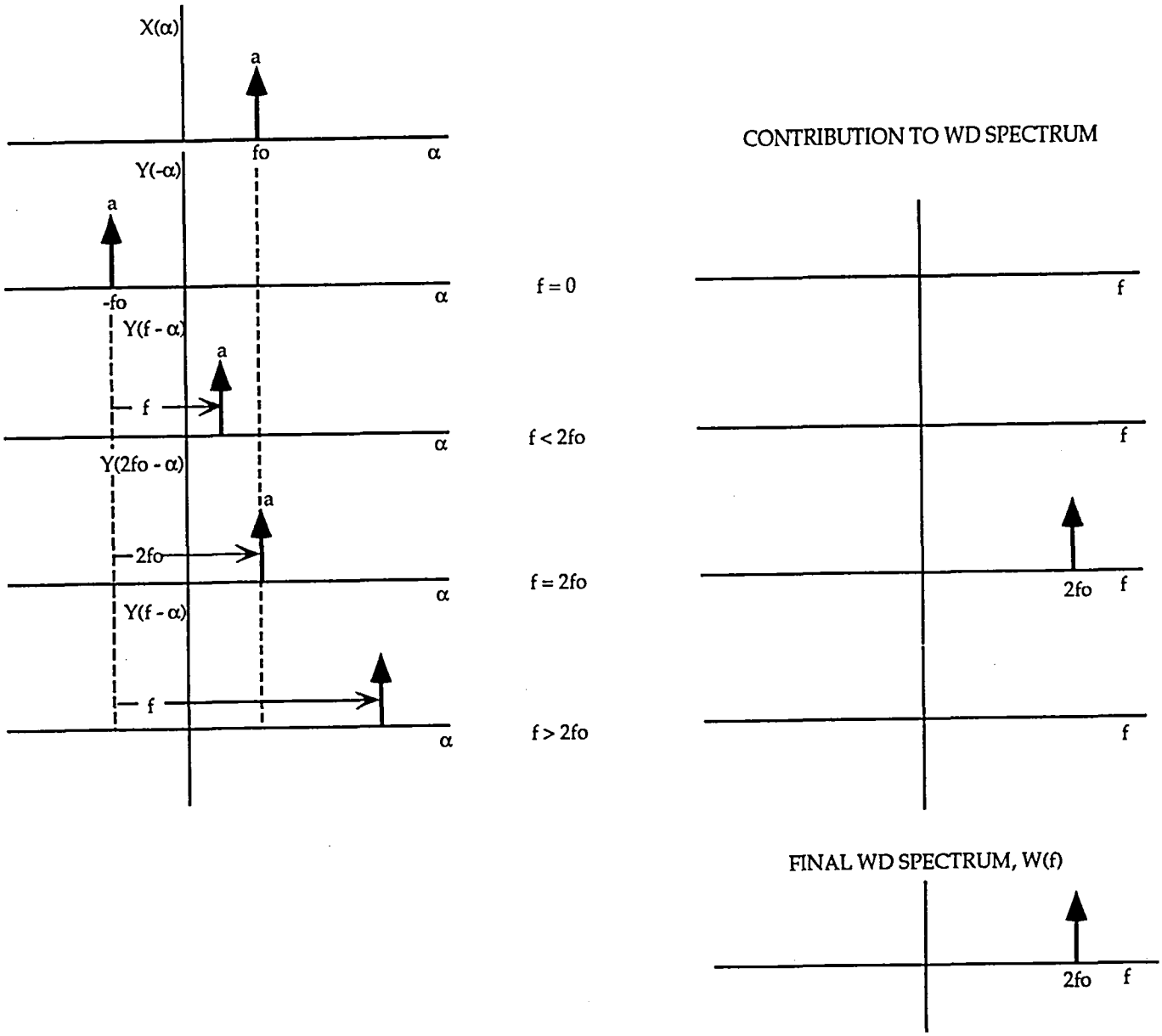

Figure 1. Graphical evaluation of case I, Wigner distribution.

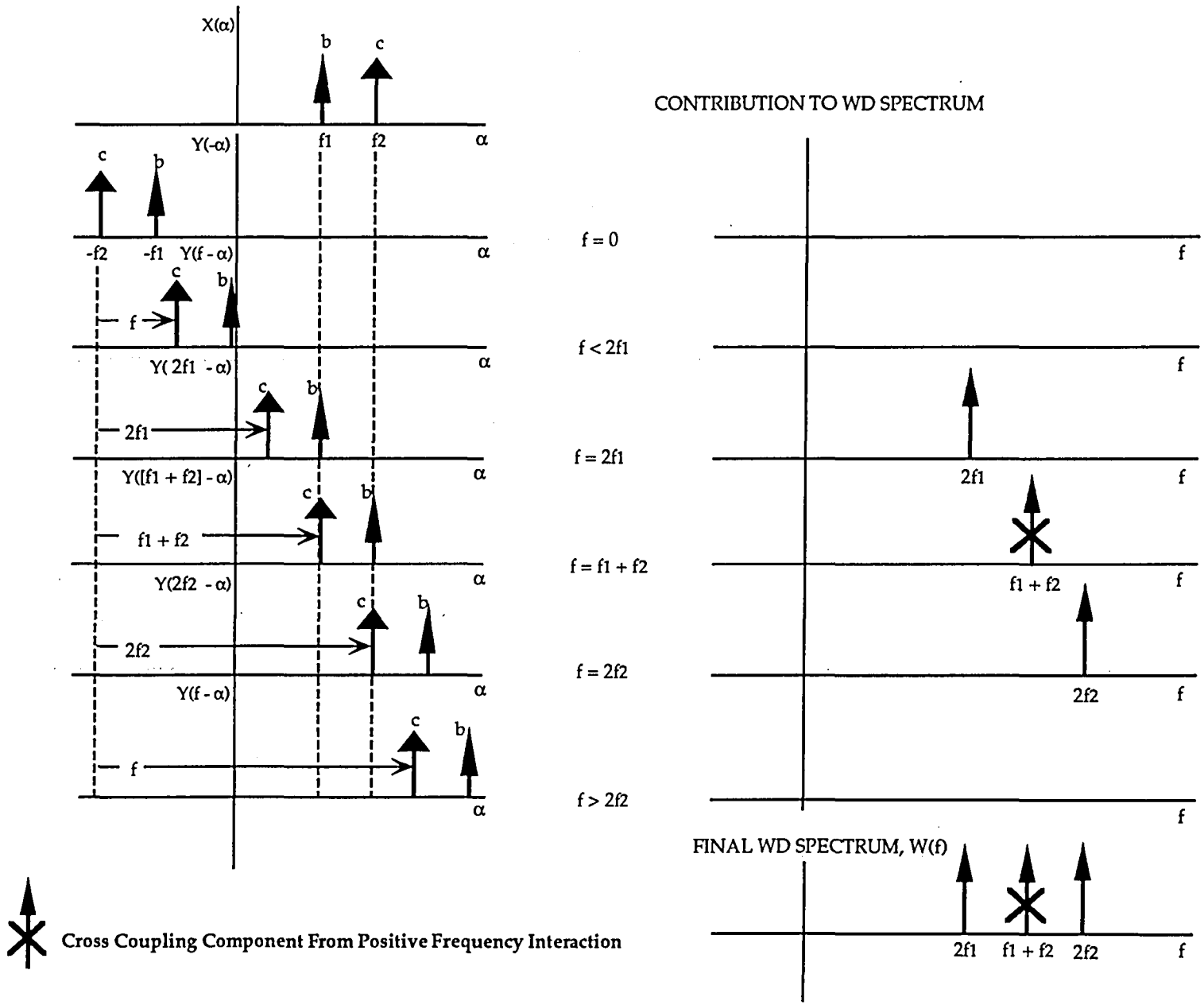

Figure 2. Graphical evaluation of case II, Wigner distribution.

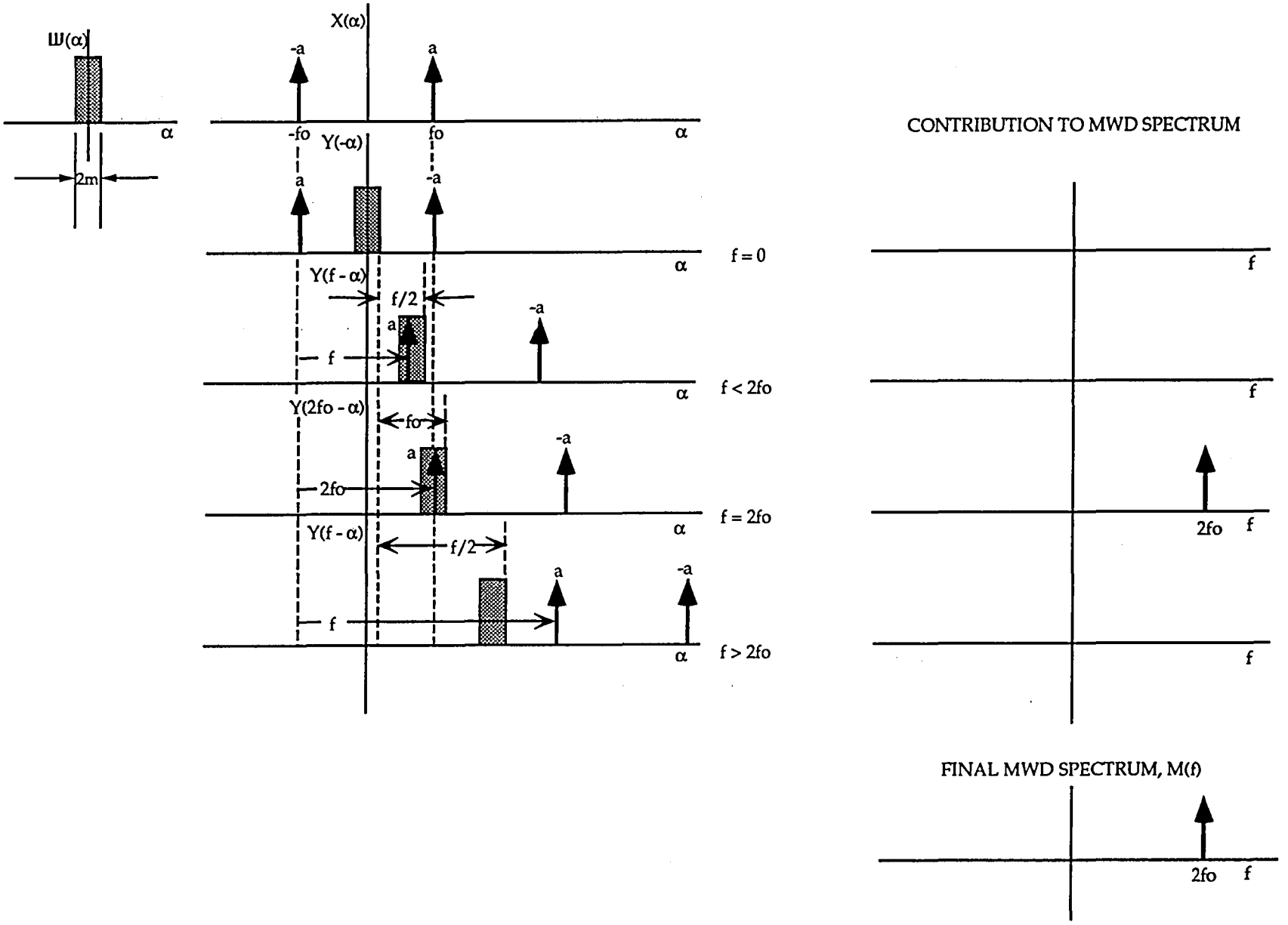

Figure 3. Graphical evaluation of case I, modified Wigner distribution.

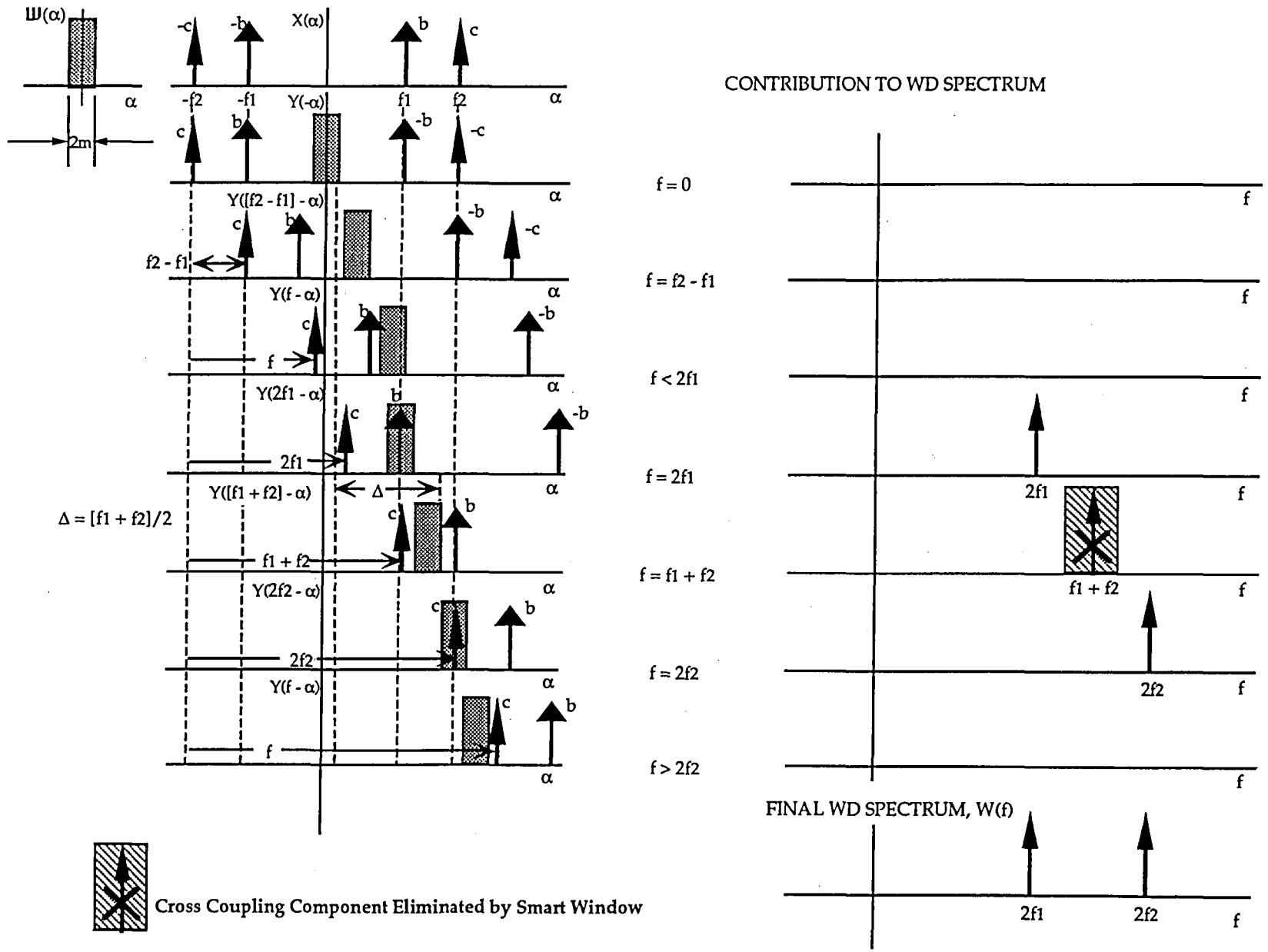

Figure 4. Graphical evaluation of case II, modified Wigner distribution.

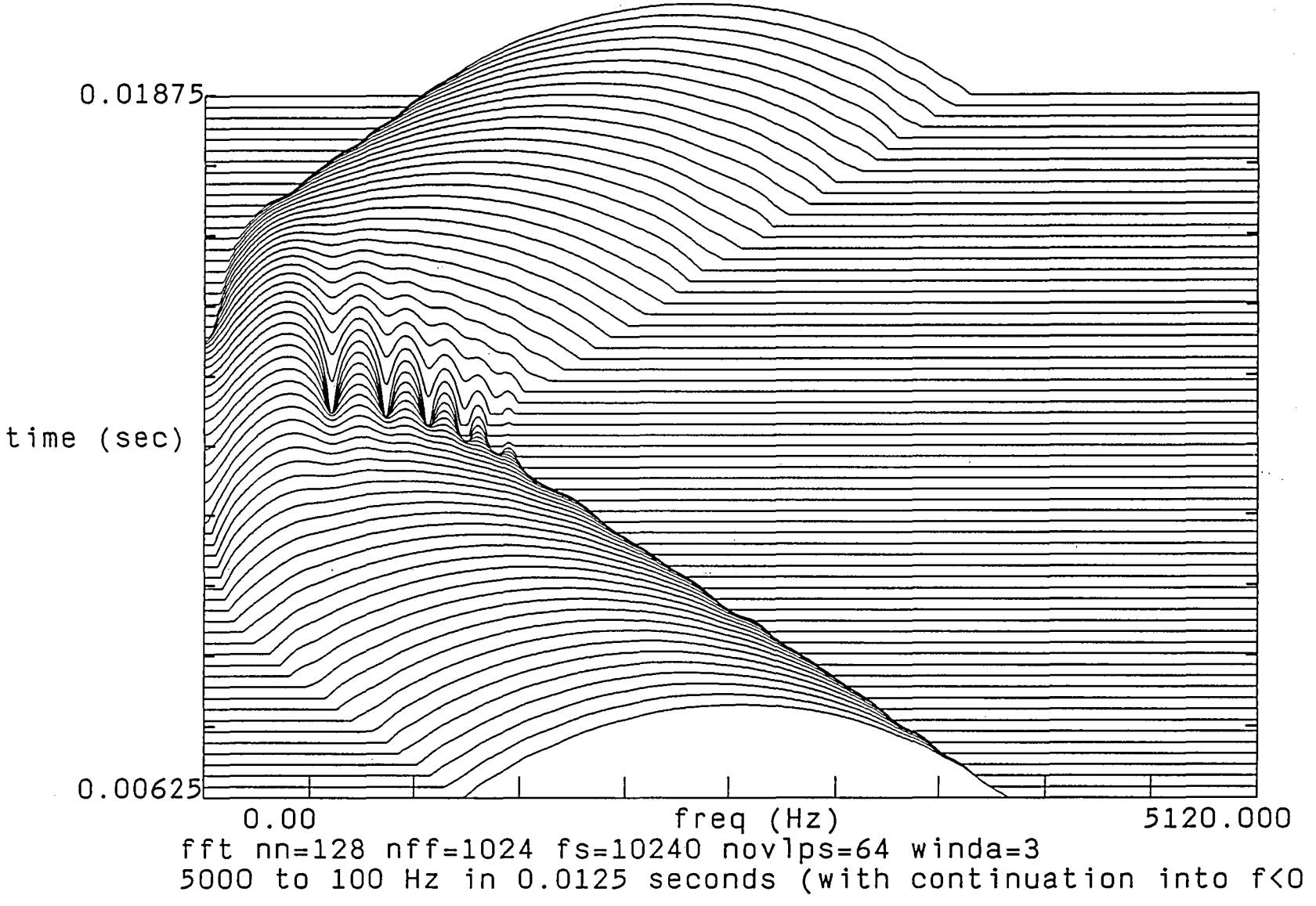
0.01875
time (sec)
0.00625
0.00
freq (Hz)
5120.000
fft nn=128 nff=1024 fs=10240 novlps=64 winda=3
5000 to 100 Hz in 0.0125 seconds (with continuation into f<0

Figure 5.

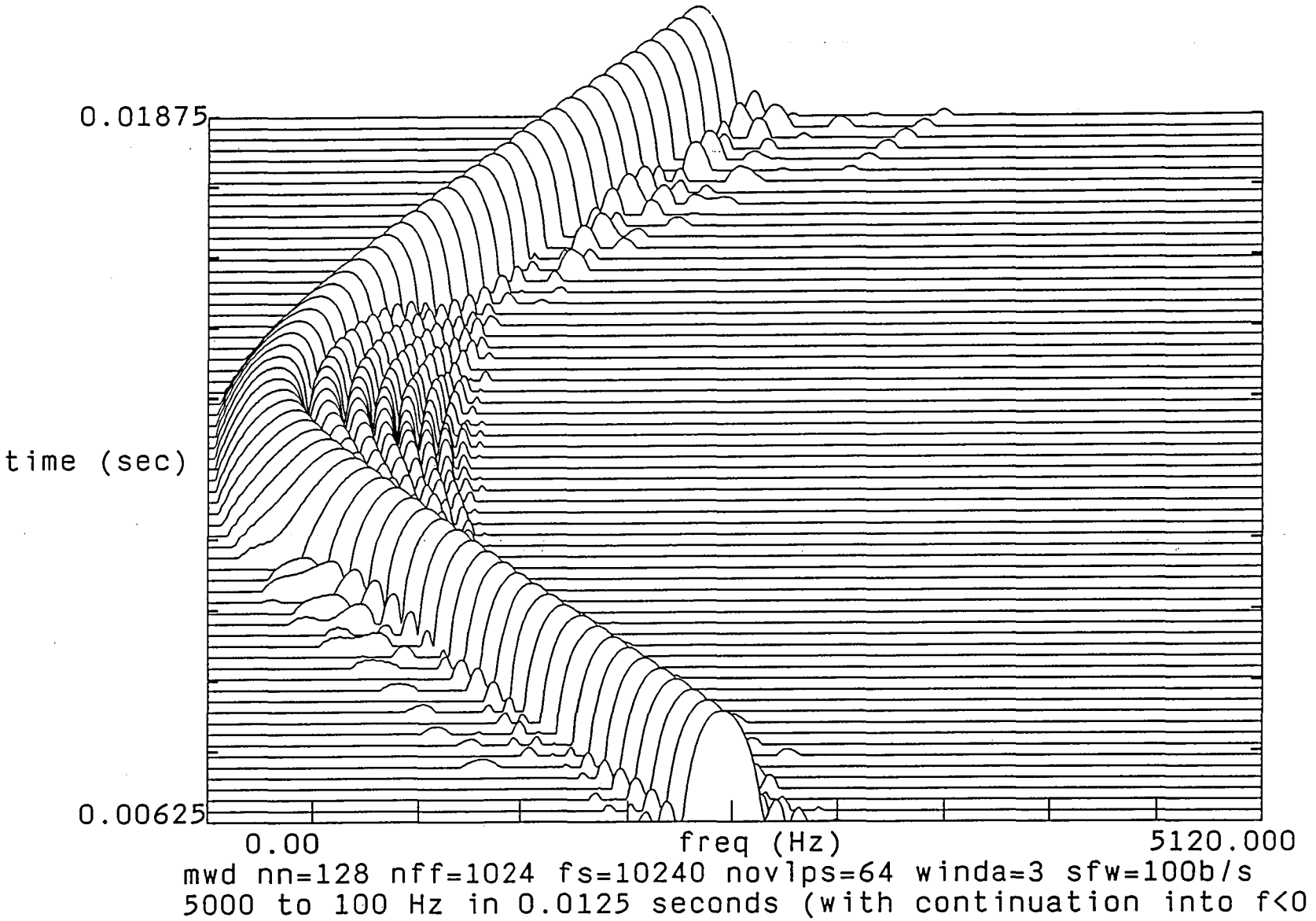
0.01875
time (sec)
0.00625
0.00
freq (Hz)
5120.000
mwd nn=128 nff=1024 fs=10240 novlps=64 winda=3 sfw=100b/s
5000 to 100 Hz in 0.0125 seconds (with continuation into f<0

Figure 6.

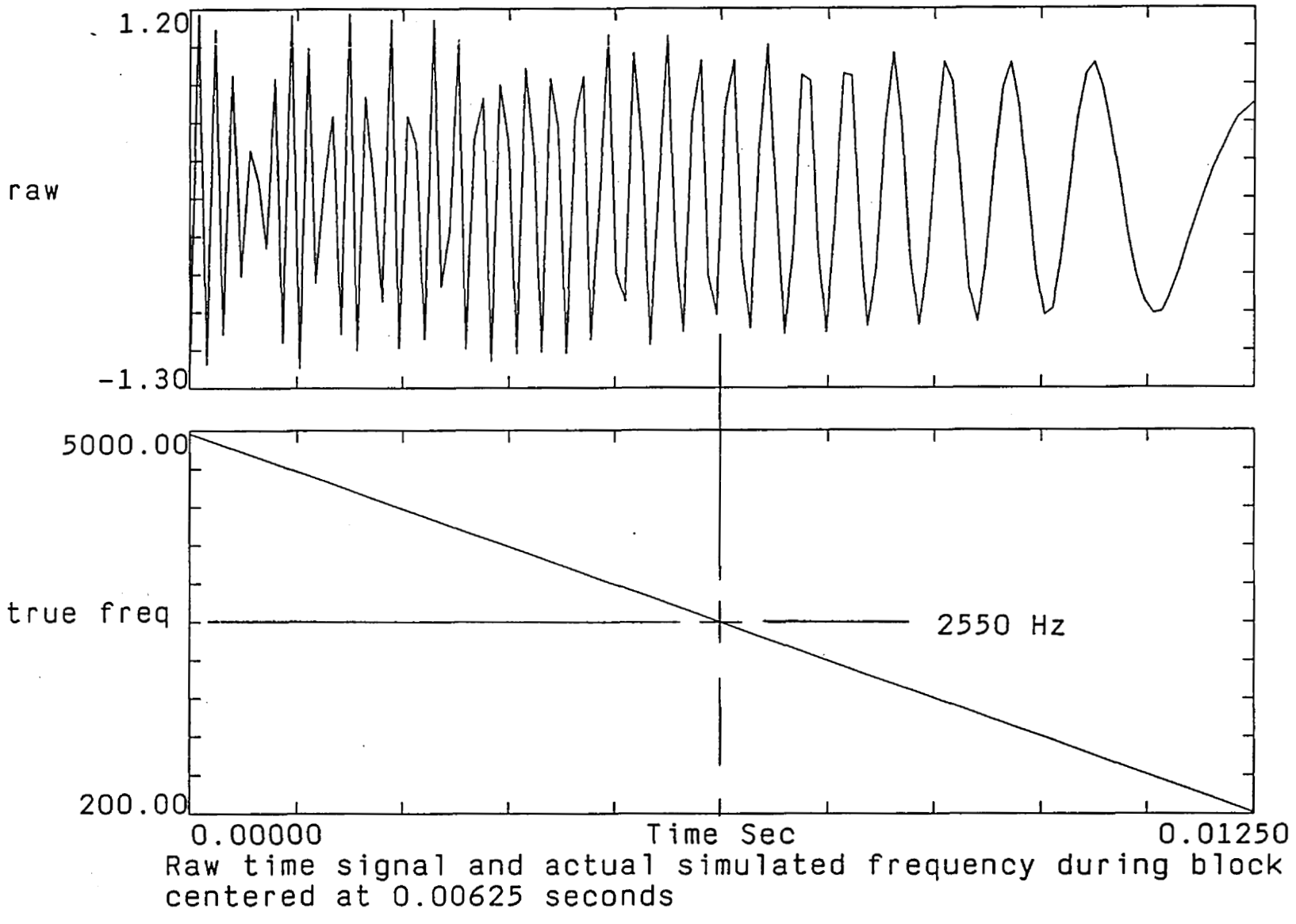
1.20
raw
-1.30
5000.00
true freq
2550 Hz
200.00
0.00000
Time Sec
0.01250
Raw time signal and actual simulated frequency during block
centered at 0.00625 seconds

Figure 7.

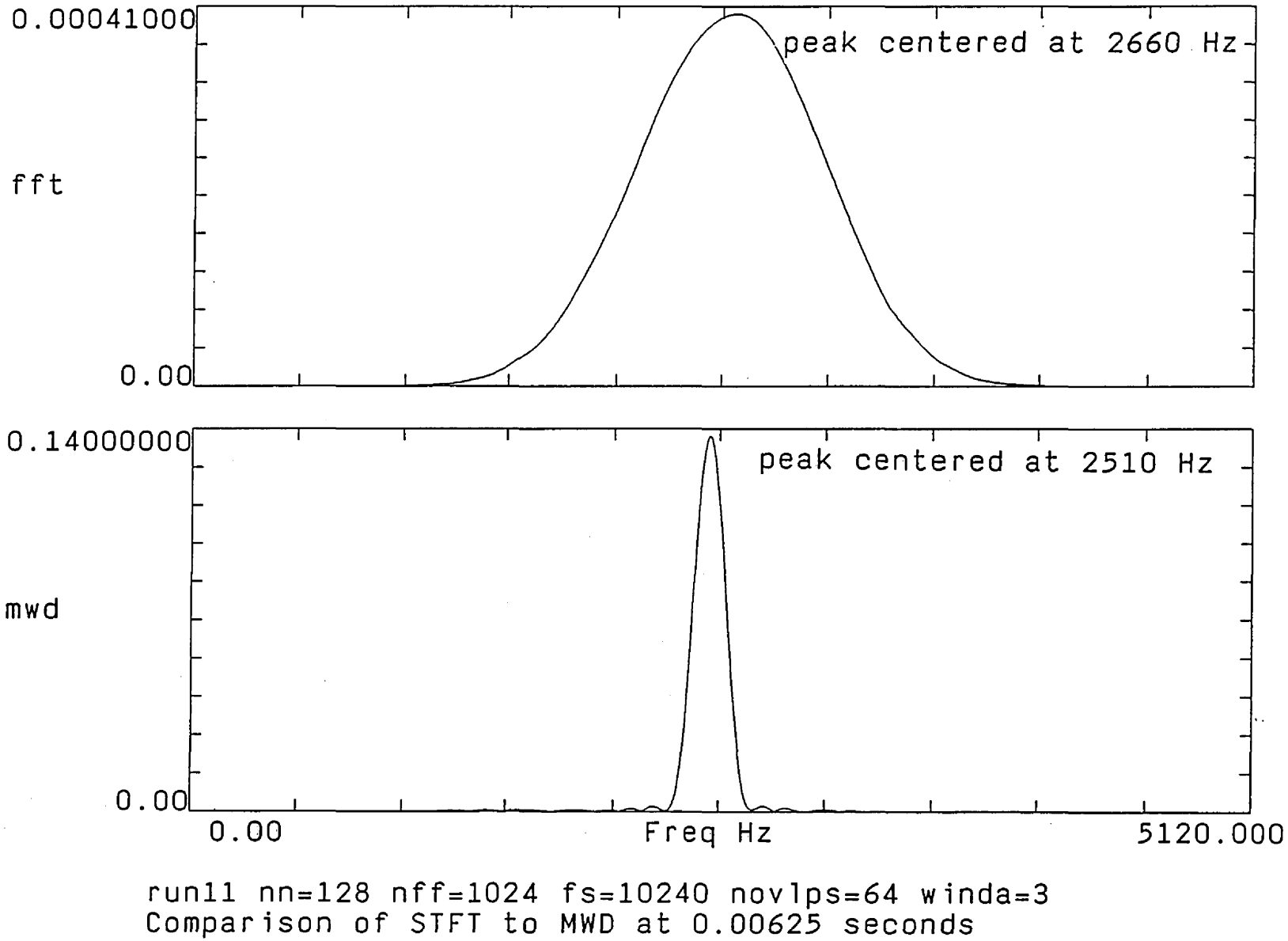
0.00041000
fft
0.00
peak centered at 2660 Hz
0.14000000
mwd
0.00
peak centered at 2510 Hz
0.00
Freq Hz
5120.000
run11 nn=128 nff=1024 fs=10240 novlps=64 winda=3
Comparison of STFT to MWD at 0.00625 seconds

Figure 8.

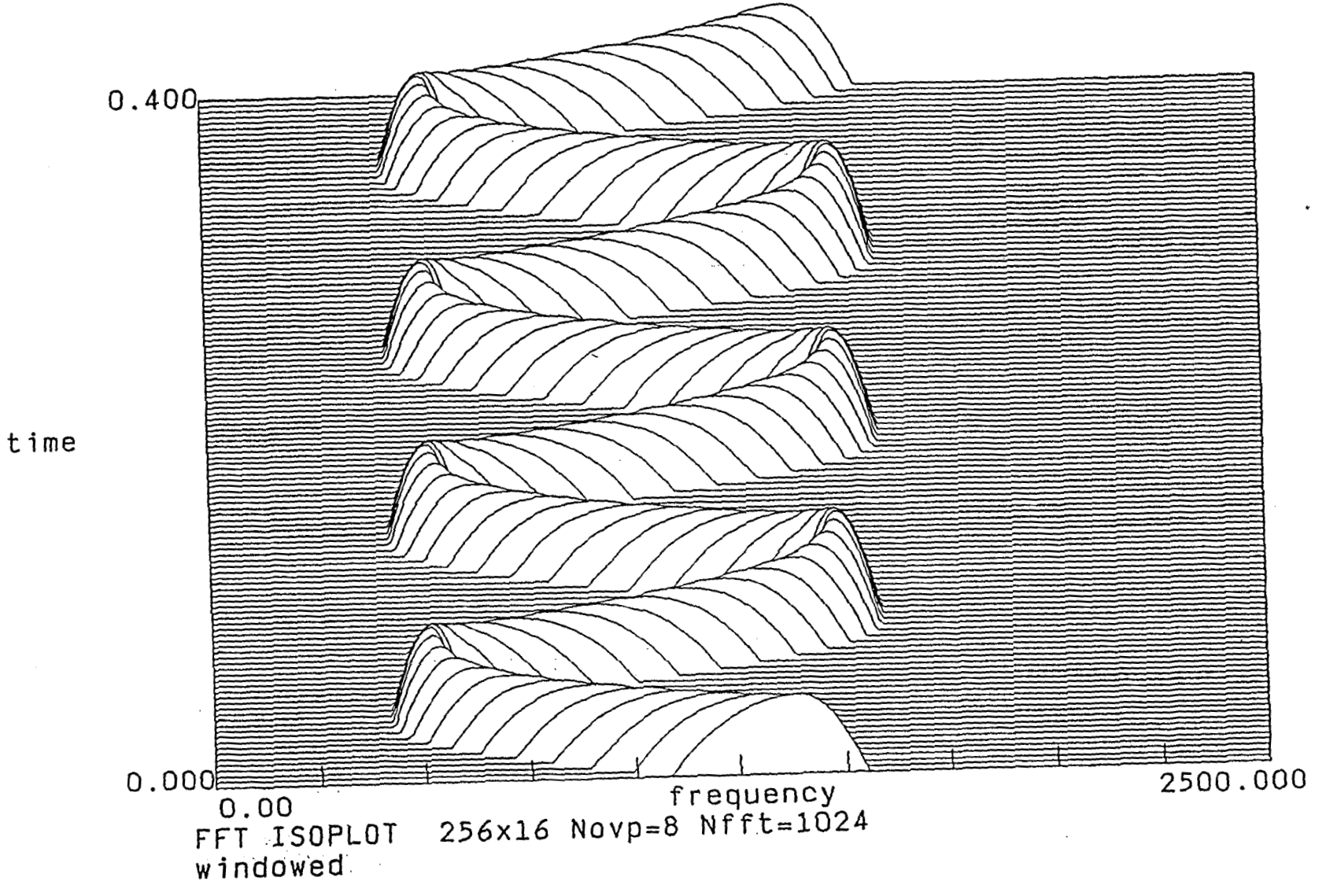
0.400
time
0.000
0.00
frequency
2500.000
FFT ISOPLOT 256x16 Novp=8 Nfft=1024
windowed

Figure 9.

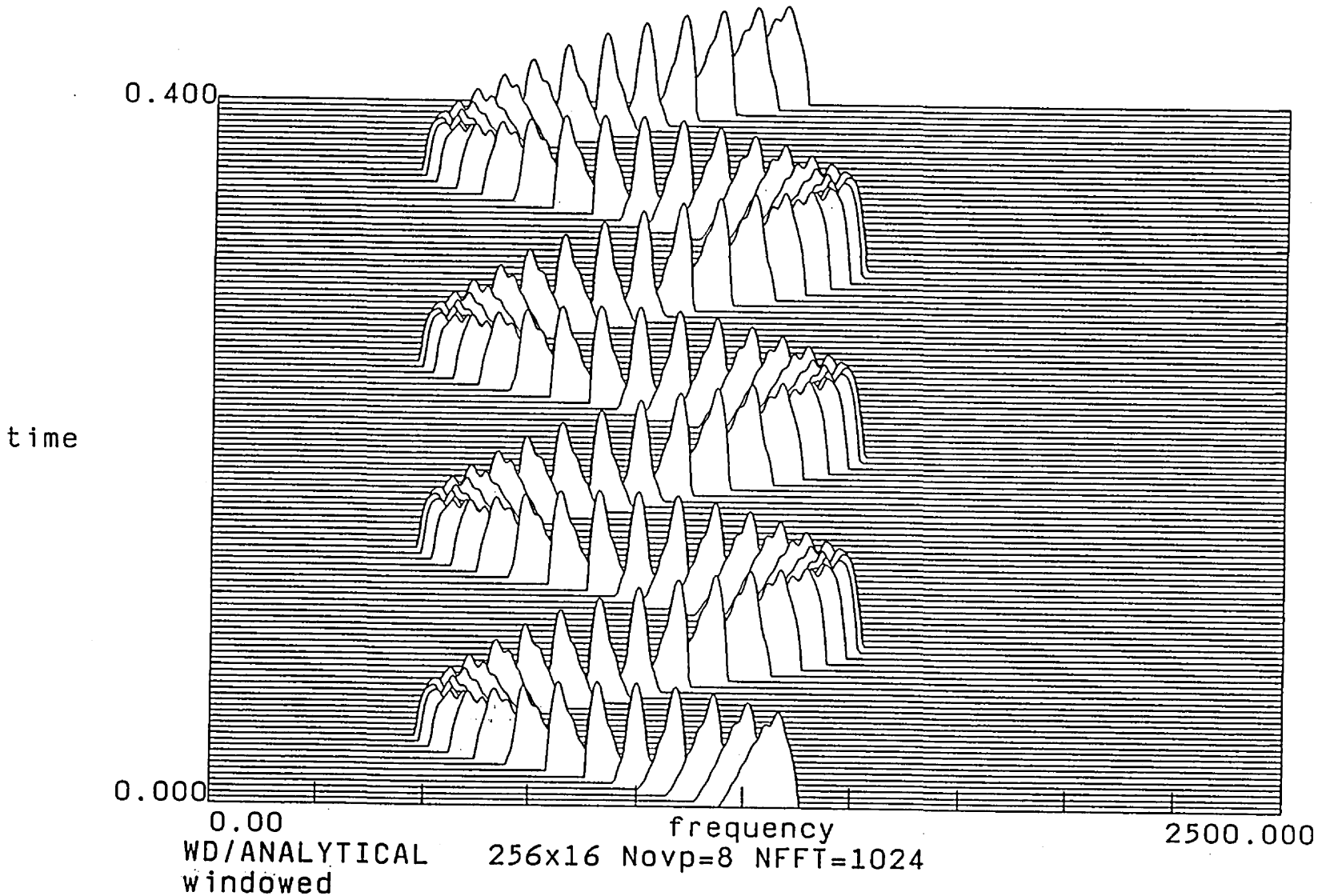
0.400
time
0.000
0.00
frequency
2500.000
WD/ANALYTICAL
windowed
256x16 Novp=8 NFFT=1024

Figure 10.

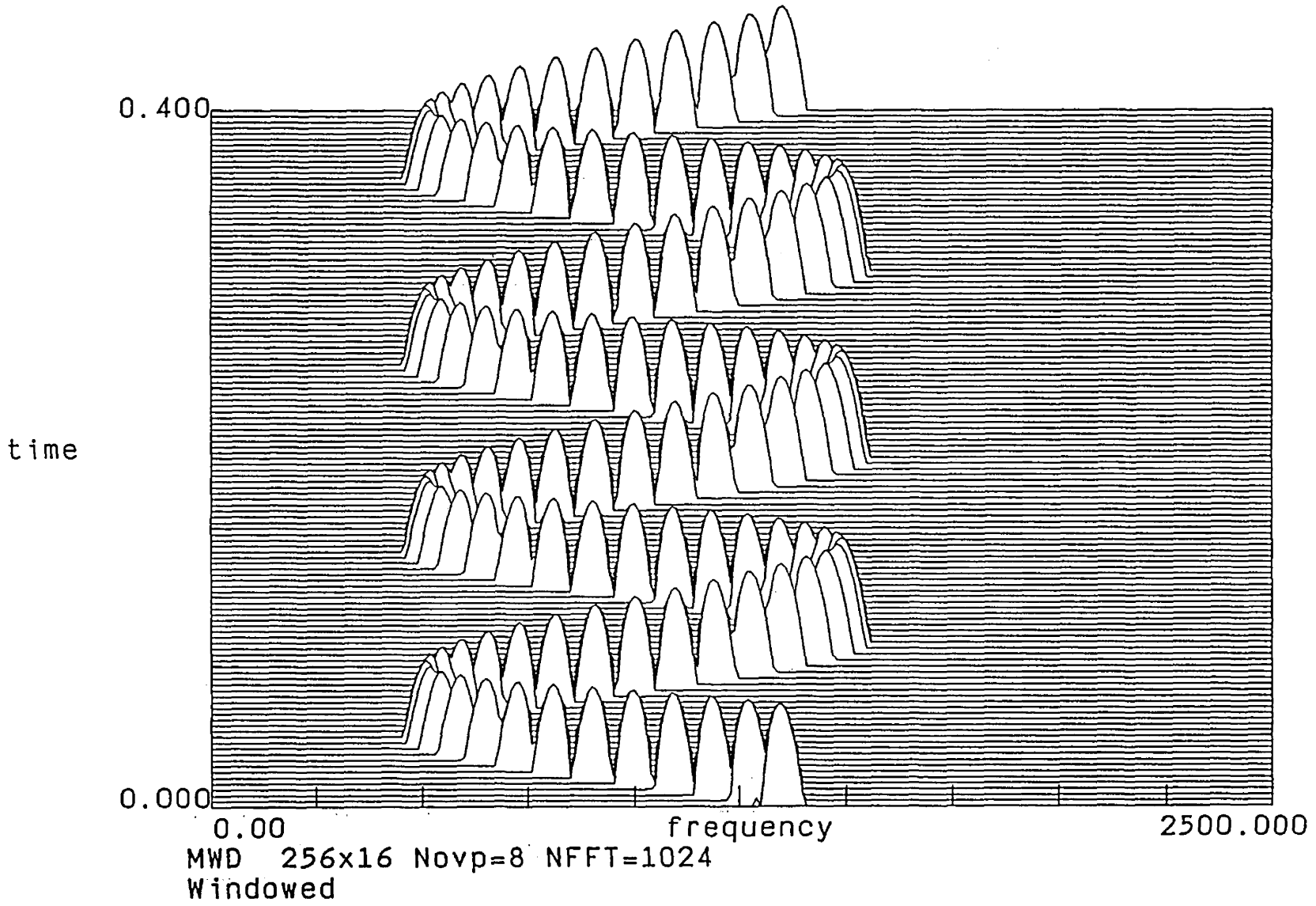
0.400
time
0.000
0.00
frequency
2500.000
MWD 256x16 Novp=8 NFFT=1024
Windowed

Figure 11.

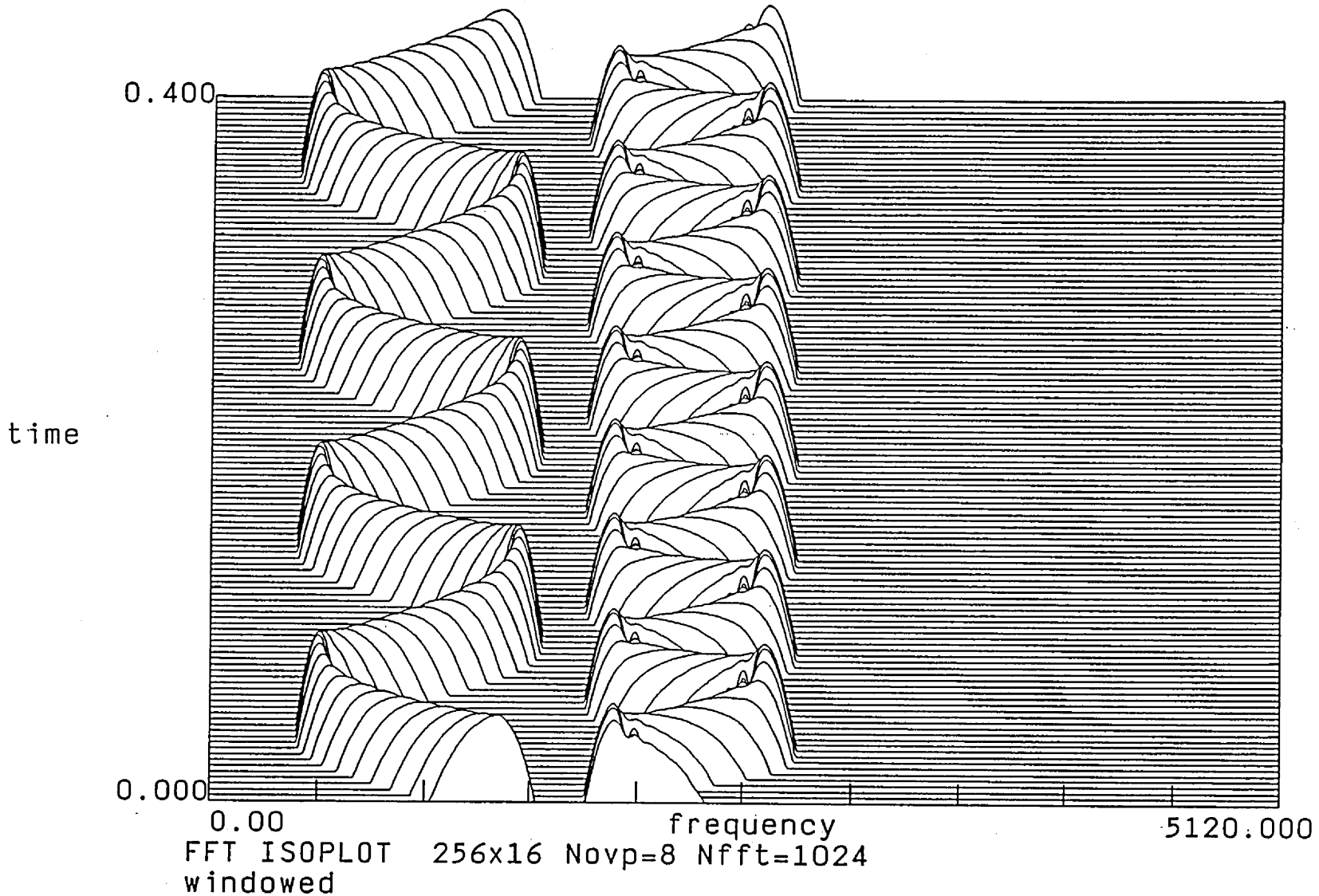
0.400
time
0.000
0.00
frequency
5120.000
FFT ISOPLOT 256x16 Novp=8 Nfft=1024
windowed

Figure 12.

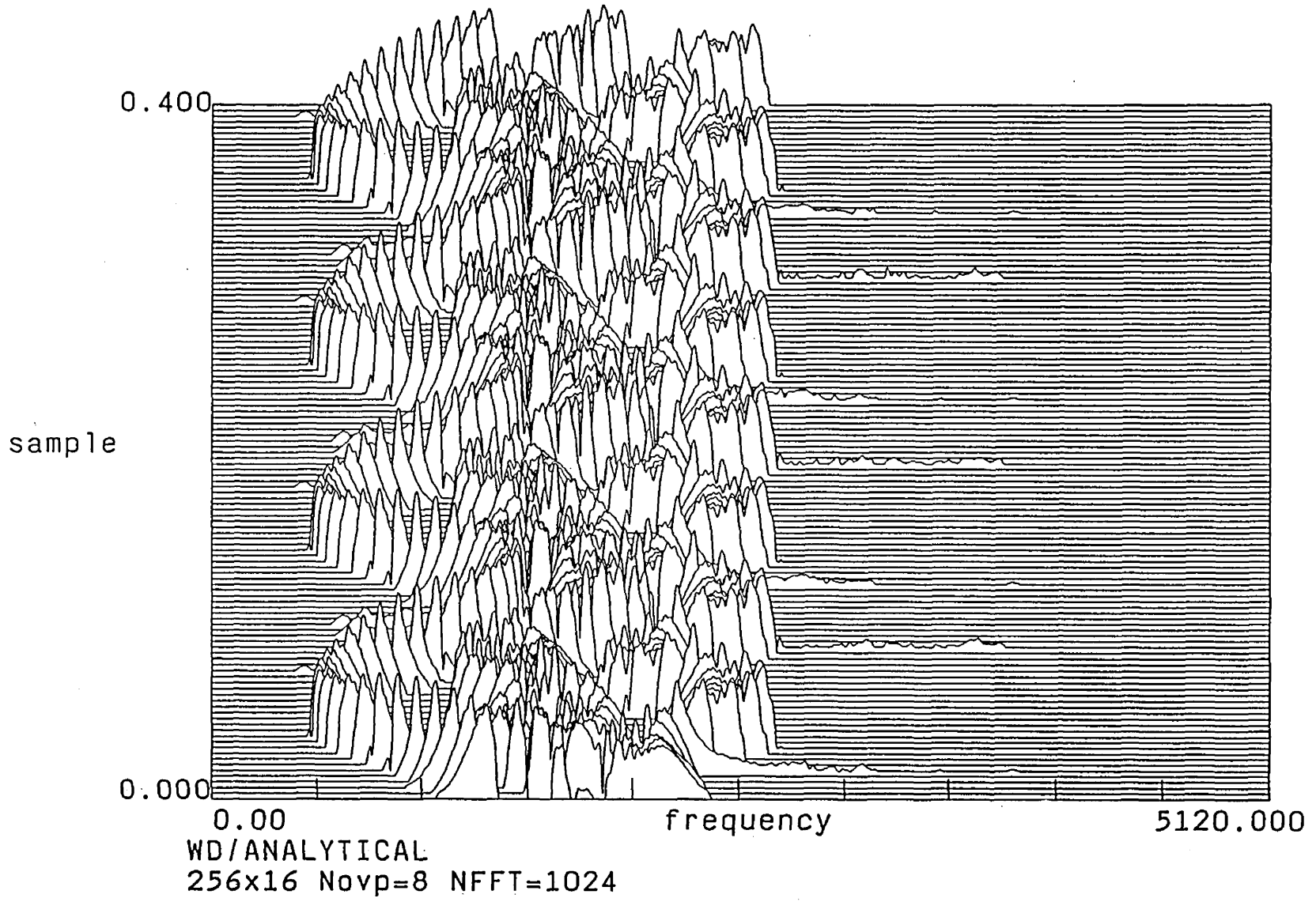
0.400
sample
0.000
0.00
frequency
5120.000
WD/ANALYTICAL
256x16 Novp=8 NFFT=1024

Figure 13.

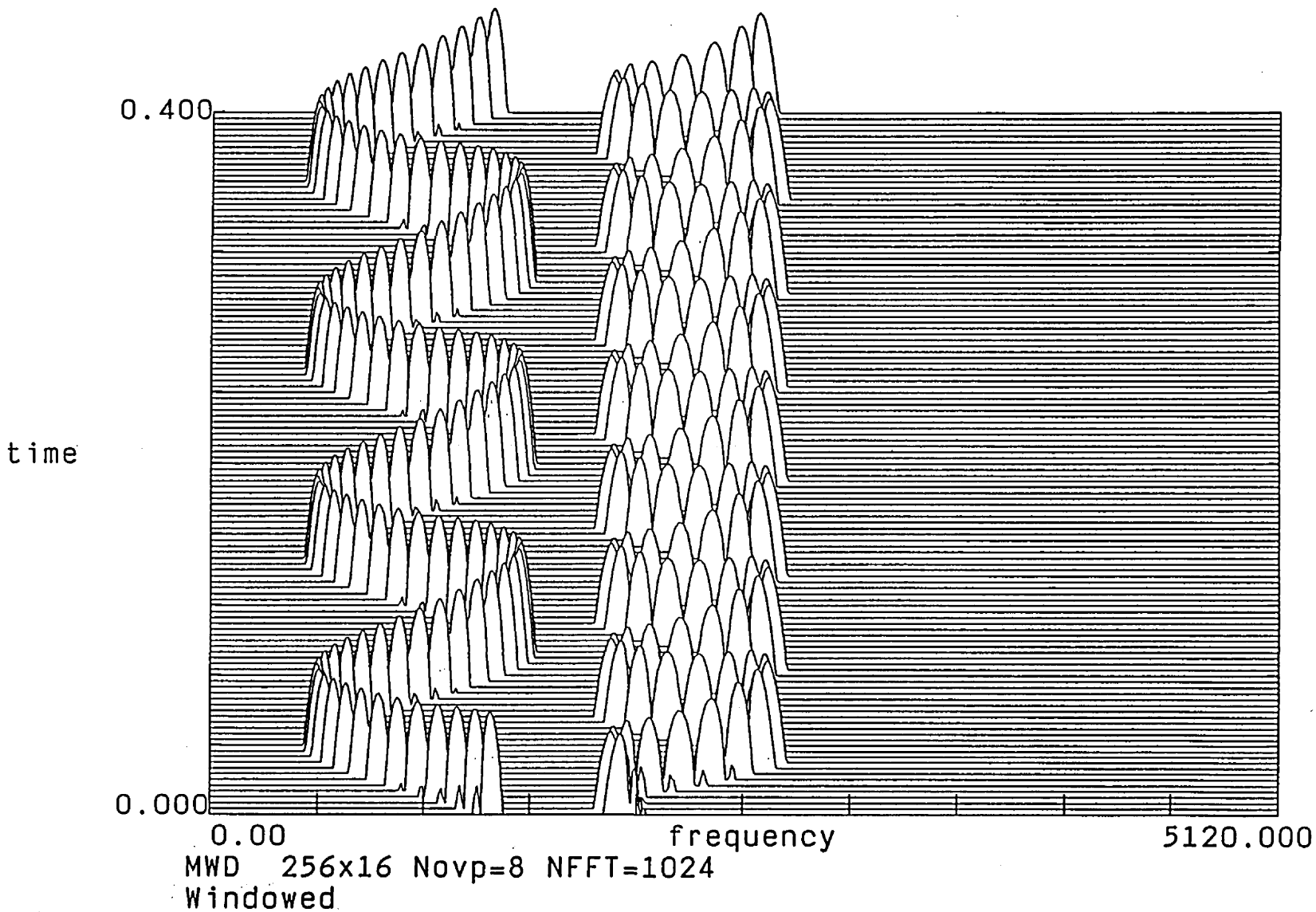
0.400
time
0.000
0.00
frequency
5120.000
MWD 256x16 Novp=8 NFFT=1024
Windowed

Figure 14.

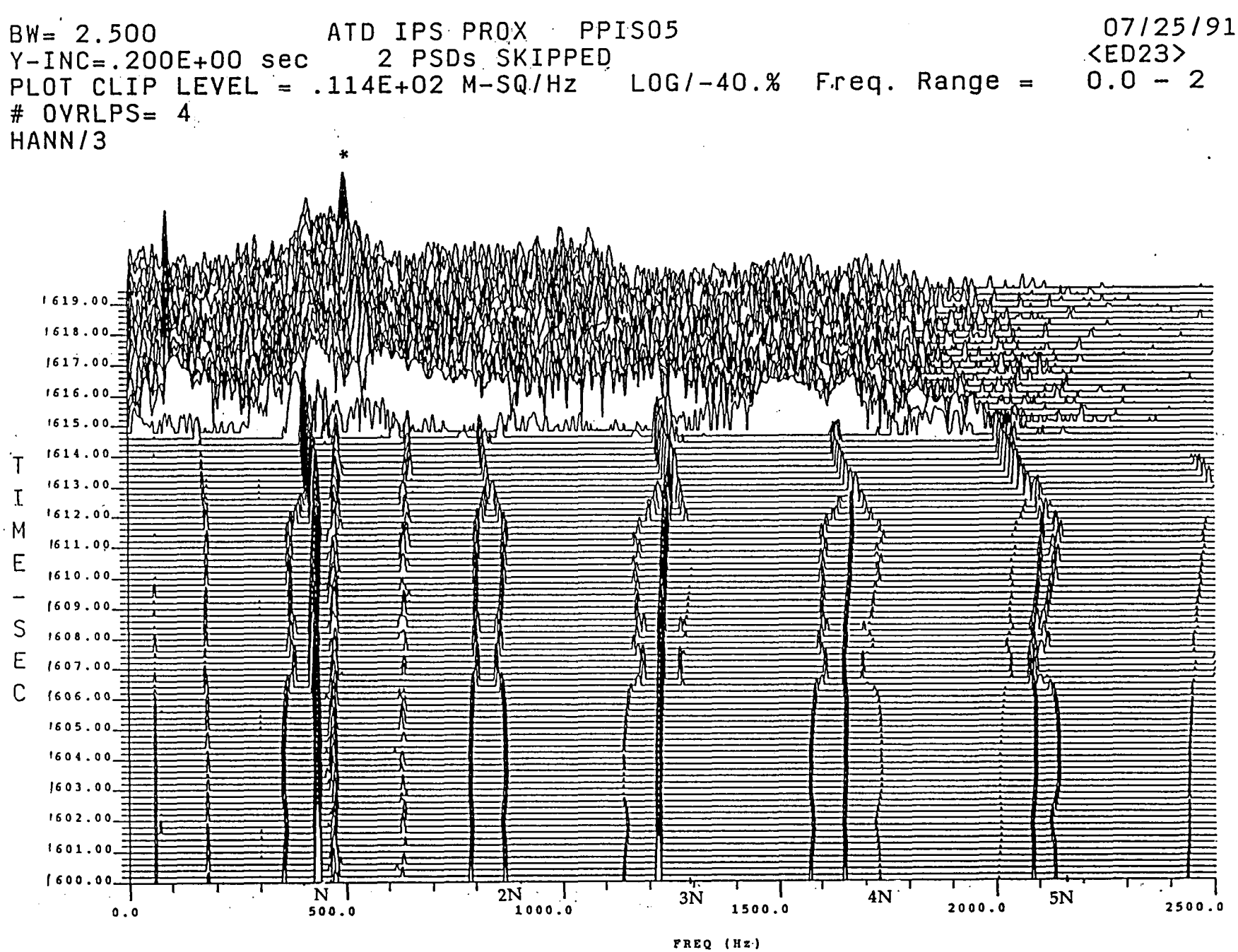
BW= 2.500
ATD IPS PROX PPIS05
07/25/91
Y-INC=.200E+00 sec
2 PSDs SKIPPED
<ED23>
PLOT CLIP LEVEL = .114E+02 M-SQ/Hz
LOG/-40.%
Freq. Range = 0.0 - 2
OVRLPS= 4
HANN/3
TIME-SEC
1619.00
1618.00
1617.00
1616.00
1615.00
1614.00
1613.00
1612.00
1611.00
1610.00
1609.00
1608.00
1607.00
1606.00
1605.00
1604.00
1603.00
1602.00
1601.00
1600.00
0.0
N
500.0
2N
1000.0
3N
1500.0
4N
2000.0
5N
2500.0
FREQ (Hz)

Figure 15.

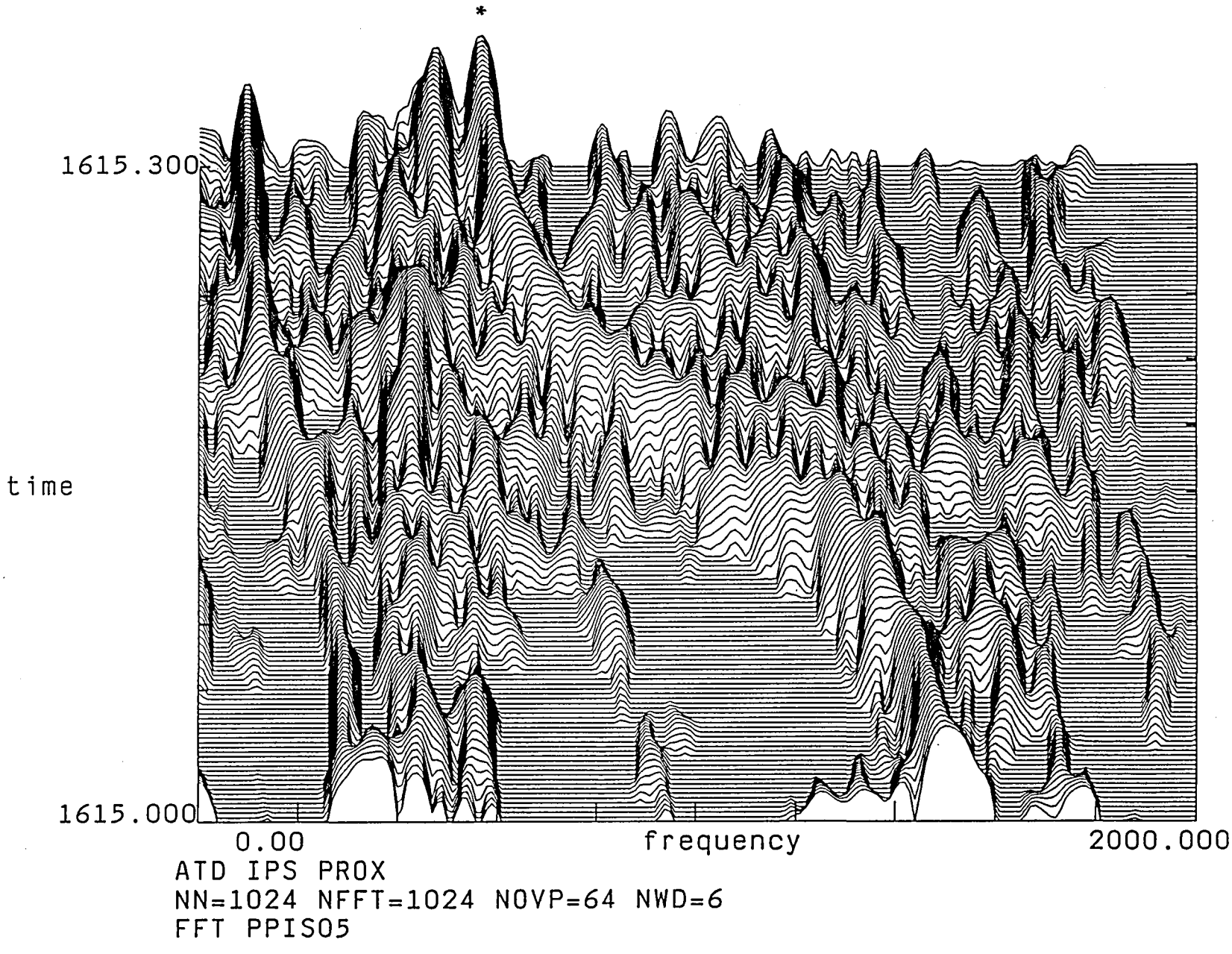
*
1615.300
time
1615.000
0.00
frequency
2000.000
ATD IPS PROX
NN=1024 NFFT=1024 NOVP=64 NWD=6
FFT PPIS05

Figure 16.

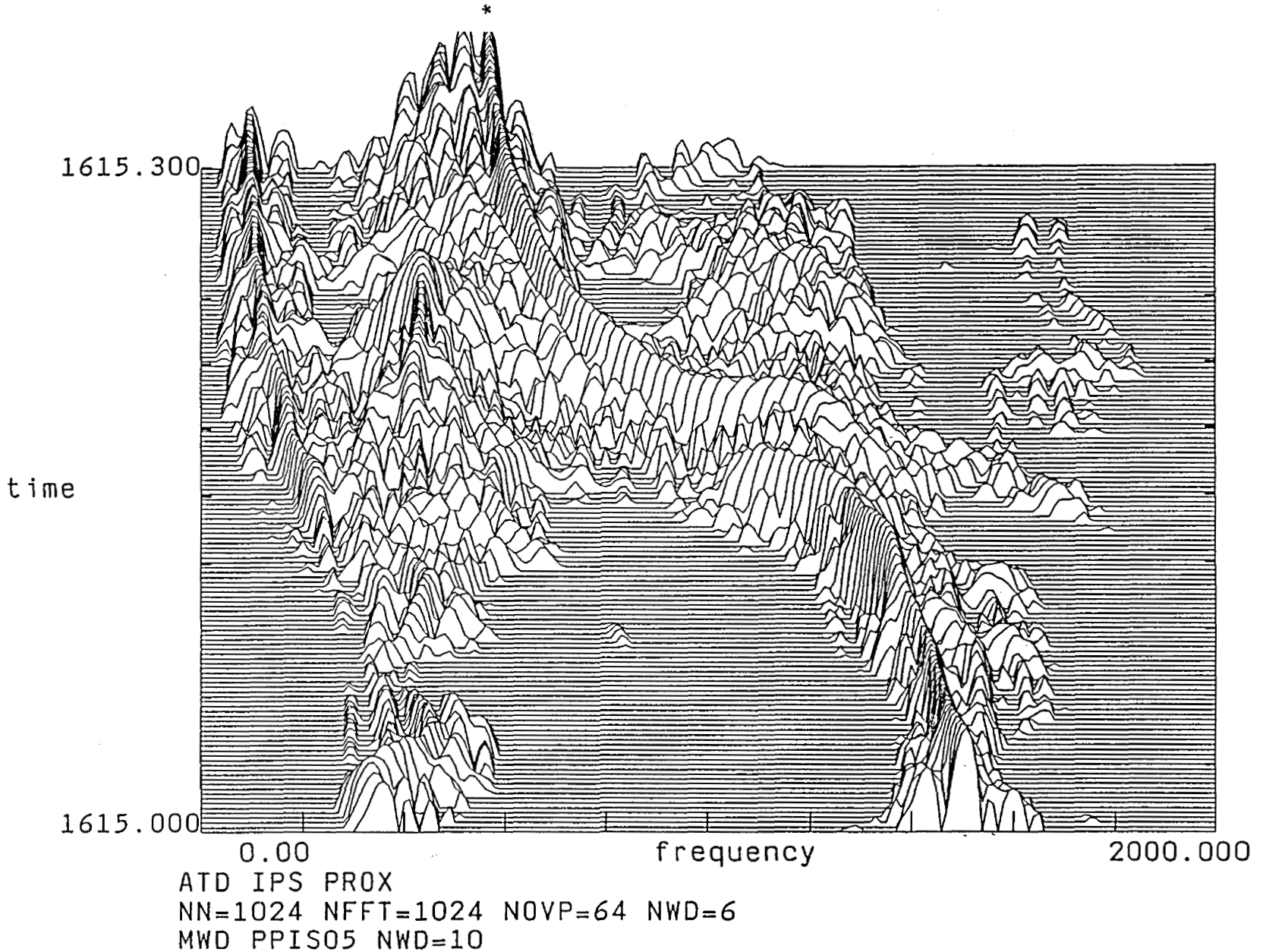
*
1615.300
time
1615.000
0.00
frequency
2000.000
ATD IPS PROX
NN=1024 NFFT=1024 NOVP=64 NWD=6
MWD PPIS05 NWD=10

Figure 17.

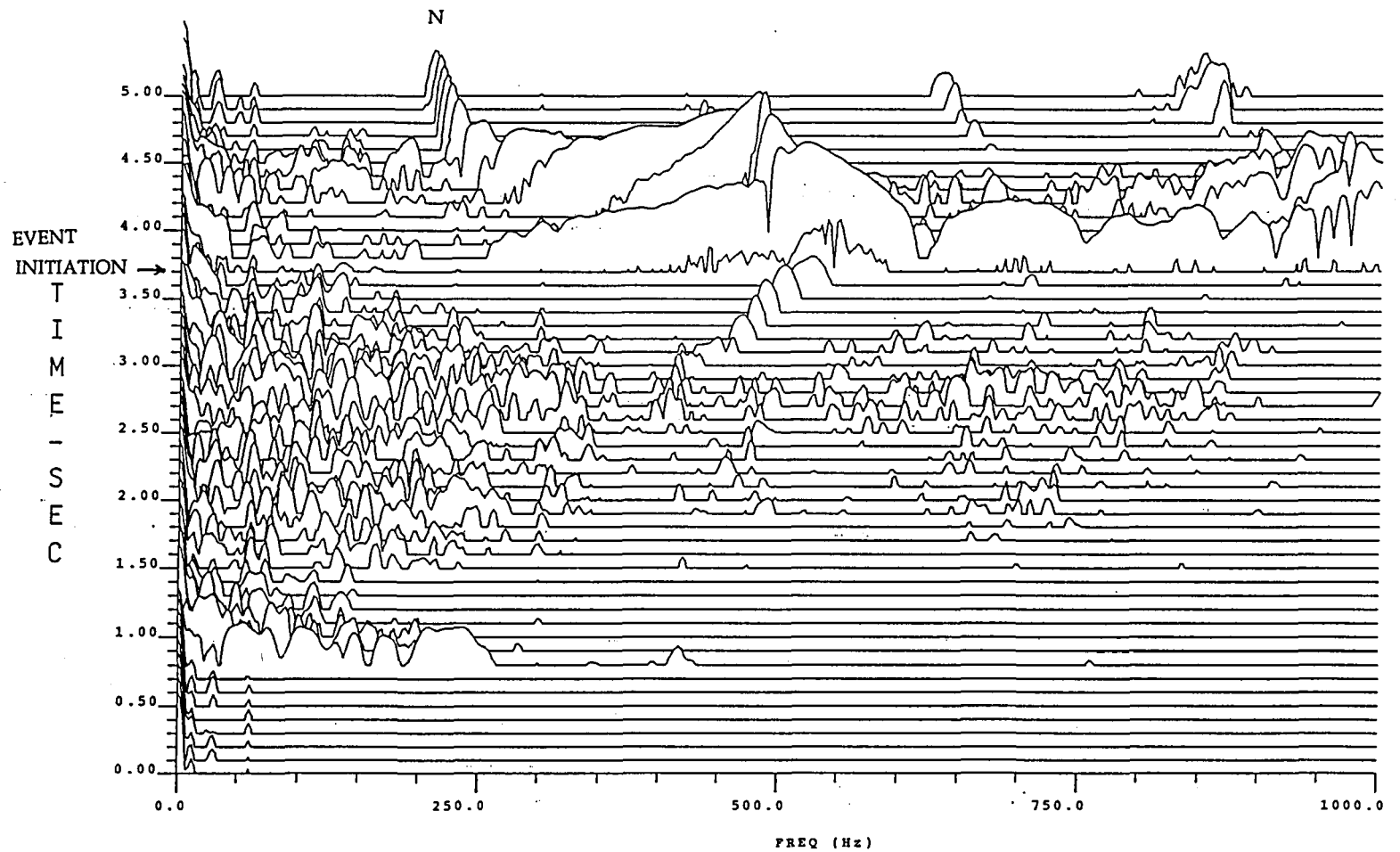
BW= 2.500 09010666 HPFP RAD 96 11/12/91
Y-INC=.100E+00 sec <ED23>
PLOT CLIP LEVEL = .285E+03 G-SQ/Hz LOG/-25.% Freq. Range = 0.0 - 1
OVRLPS= 4
HANN/3
N
EVENT
INITIATION
TIME-SEC
5.00
4.50
4.00
3.50
3.00
2.50
2.00
1.50
1.00
0.50
0.00
0.0
250.0
500.0
750.0
1000.0
FREQ (Hz)

Figure 18.

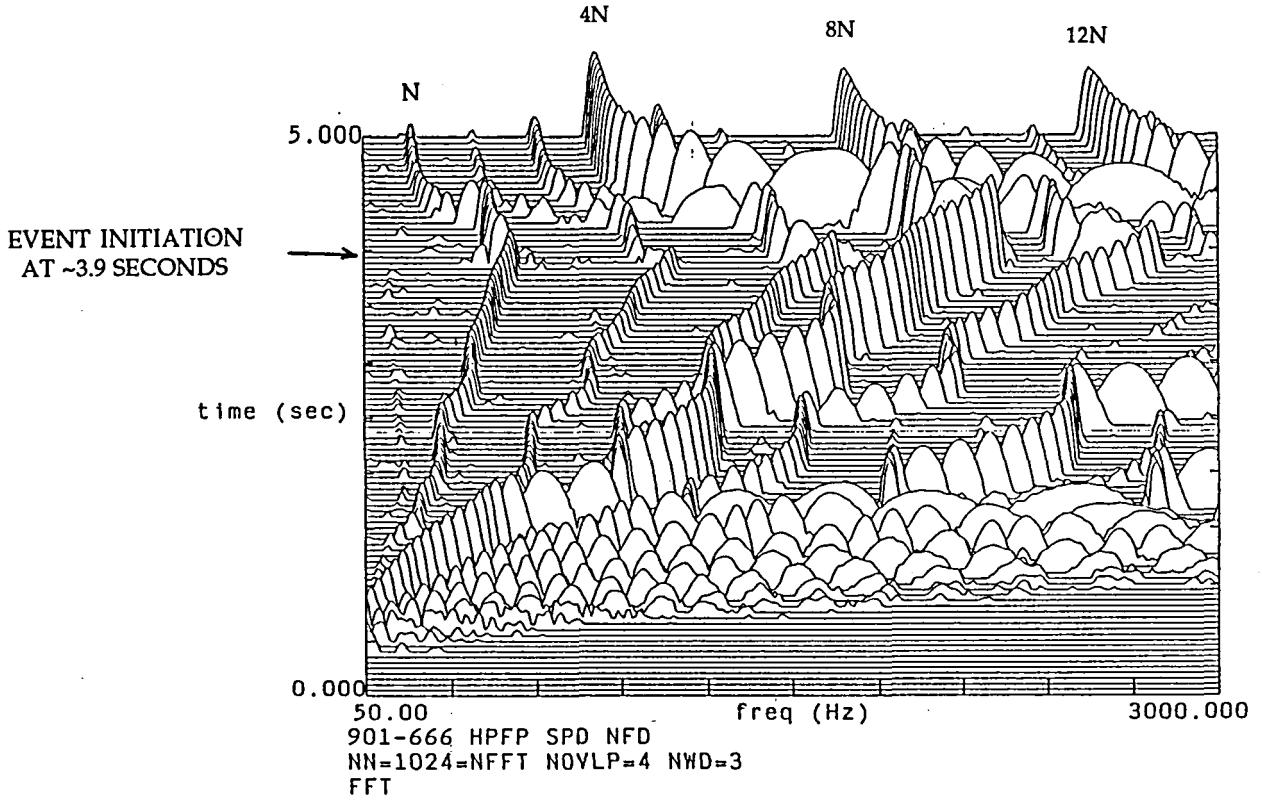
4N
8N
12N
N
5.000
EVENT INITIATION
AT ~3.9 SECONDS
time (sec)
0.000
50.00
freq (Hz)
3000.000
901-666 HPFP SPD NFD
NN=1024=NFFT NOVLP=4 NWD=3
FFT

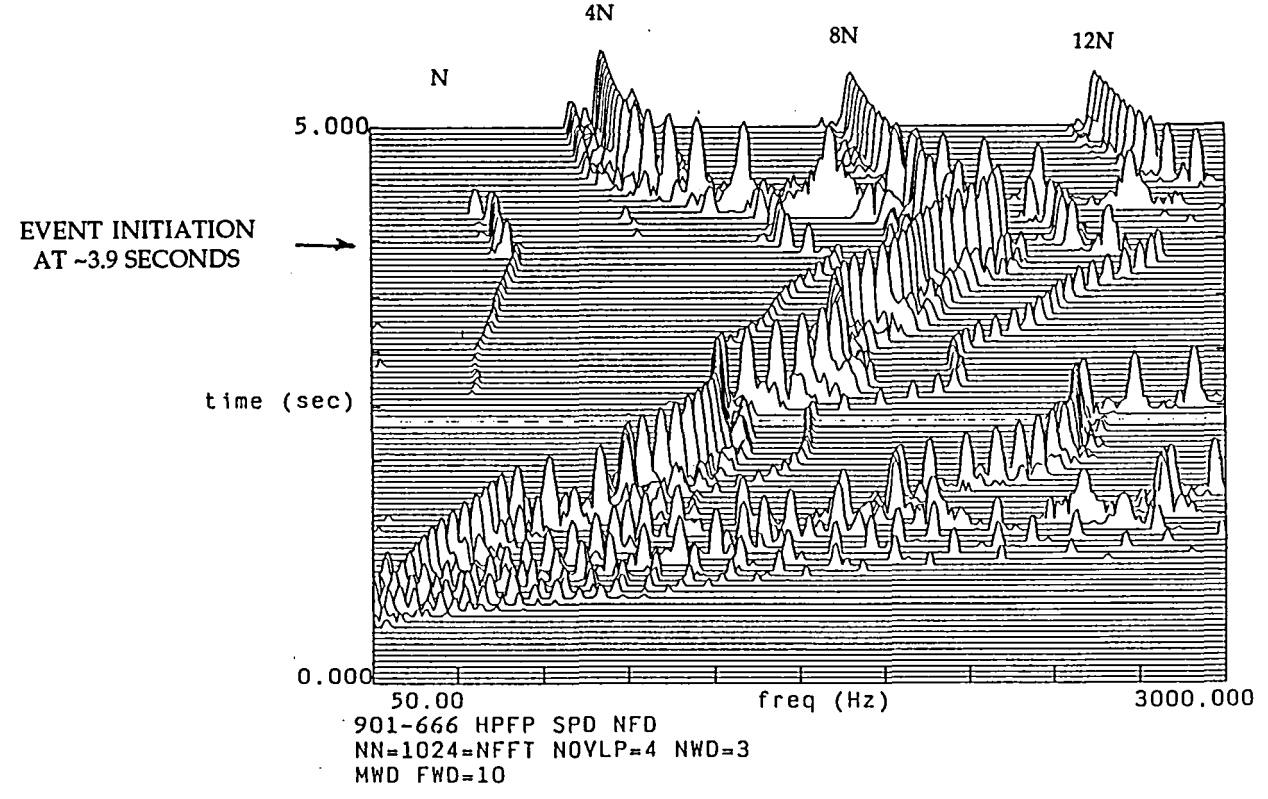
4N
8N
12N
N
5.000
EVENT INITIATION
AT ~3.9 SECONDS
time (sec)
0.000
50.00
freq (Hz)
3000.000
901-666 HPFP SPD NFD
NN=1024=NFFT NOVLP=4 NWD=3
MWD FWD=10

Figure 19.

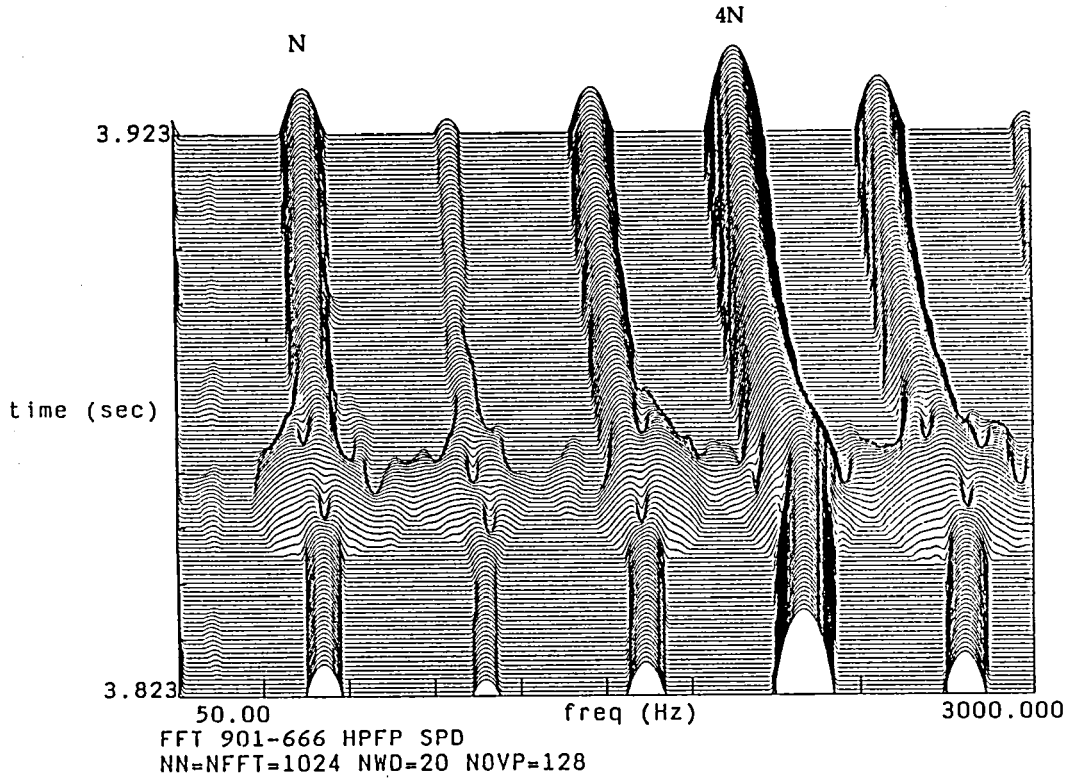
4N
N
3.923
time (sec)
3.823
50.00
freq (Hz)
3000.000
FFT 901-666 HPFP SPD
NN=NFFT=1024 NWD=20 NOVP=128

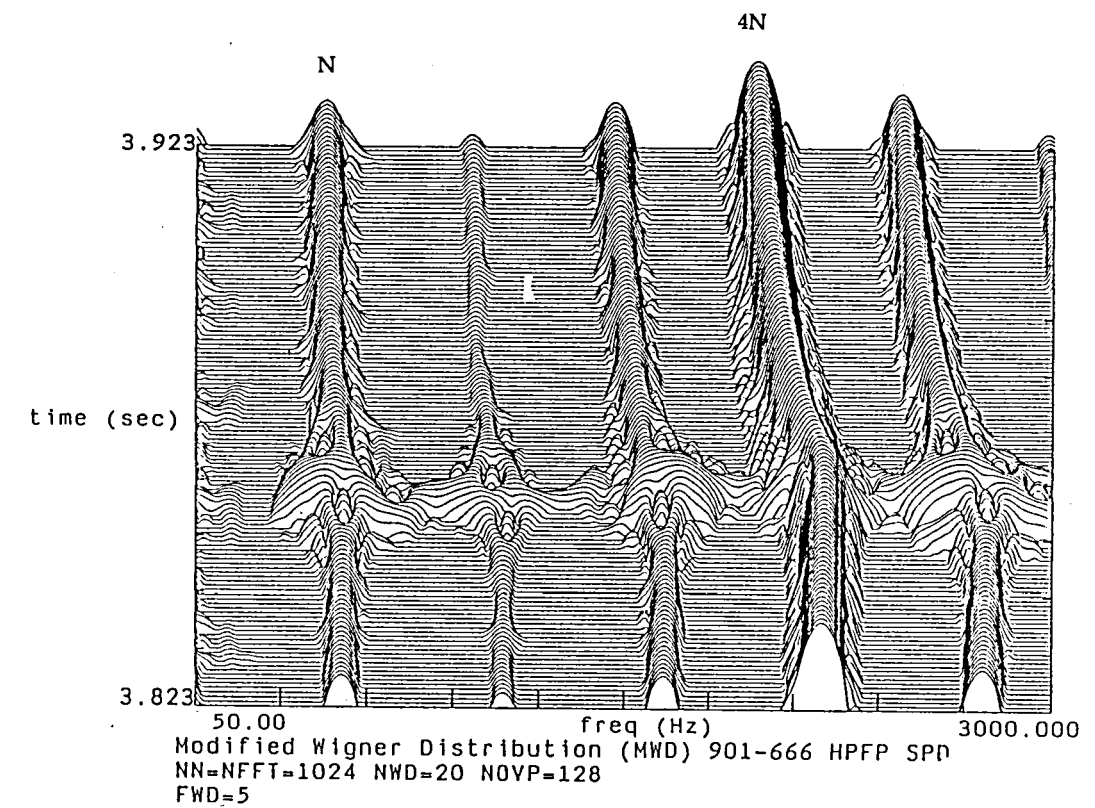
4N
N
3.923
time (sec)
3.823
50.00
freq (Hz)
3000.000
Modified Wigner Distribution (MWD) 901-666 HPFP SPD
NN=NFFT=1024 NWD=20 NOVP=128
FWD=5

Figure 20.

REFERENCES

1. Wigner, E.: "On the Quantum Correction for Thermodynamic Equilibrium." Phys. Rev. 40, 1932, pp. 749–759.

2. Claasen, T.A.C.M., and Mecklenbrauker, W.F.G.: "The Wigner Distribution—A Tool For Time-Frequency Signal Analysis." Philips Journal of Research, vol. 35, pp. 217–250, 276–300, 372–389.

3. Boashash, B., and Black, P.: "An Efficient Real-Time Implementation of the Wigner-Ville Distribution." IEEE Transactions on Acoustics, Speech, and Signal Processing, vol. ASSP-35, No. 11, November 1987.

4. Meng, Qingfeng, and Qu, Liangsheng: "Rotating Machinery Fault Diagnosis Using Wigner Distribution." Mechanical Systems and Signal Processing, vol. 5(3), 1991, pp. 155–166.

5. Rao, P., Taylor, F., and Harrison, G.: "Real-Time Monitoring of Vibrations Using the Wigner Distribution." Sound and Vibration, May 1990.

REPORT DOCUMENTATION PAGE

Form Approved
OMB No. 0704-0188

1. AGENCY USE ONLY (Leave blank)	2. REPORT DATE	3. REPORT TYPE AND DATES COVERED
	March 1992	Technical Paper

4. TITLE AND SUBTITLE

Time-Frequency Representation of a Highly Nonstationary Signal Via the Modified Wigner Distribution

5. FUNDING NUMBERS

6. AUTHOR(S)

T.F. Zoladz, J.H. Jones, and J. Jong

7. PERFORMING ORGANIZATION NAME(S) AND ADDRESS(ES)

George C. Marshall Space Flight Center
Marshall Space Flight Center, Alabama 35812

8. PERFORMING ORGANIZATION REPORT NUMBER

M-685

9. SPONSORING/MONITORING AGENCY NAME(S) AND ADDRESS(ES)

National Aeronautics and Space Administration
Washington, DC 20546

10. SPONSORING/MONITORING AGENCY REPORT NUMBER

NASA TP-3215

11. SUPPLEMENTARY NOTES

Prepared by Structures and Dynamics Laboratory, Science and Engineering Directorate.

Zoladz and Jones: George C. Marshall Space Flight Center, Marshall Space Flight Center, AL.
Jong: Wyle Laboratories, Huntsville, AL.

12a. DISTRIBUTION/AVAILABILITY STATEMENT

Subject Category: 33

Unclassified—Unlimited

12b. DISTRIBUTION CODE

13. ABSTRACT *(Maximum 200 words)*

This report presents a new signal analysis technique called the modified Wigner distribution (MWD). The MWD has been developed for the Structures and Dynamics Laboratory at MSFC by Dr. Jen-Yi Jong of Wyle Laboratories. The new signal processing tool has proven very successful in determining time-frequency representations of highly nonstationary multicomponent signals in both simulation and trials involving actual space shuttle main engine high-frequency data. The MWD departs from the classic Wigner distribution (WD) in that it effectively eliminates the cross coupling among positive frequency components in a multiple component signal. This attribute of the MWD, which prevents the generation of "phantom" spectral peaks, will undoubtedly increase the utility of the WD for real-world signal analysis applications which more often than not involve multicomponent signals.

14. SUBJECT TERMS	15. NUMBER OF PAGES
Signal Processing, High Frequency	36
	16. PRICE CODE: A03

17. SECURITY CLASSIFICATION OF REPORT	18. SECURITY CLASSIFICATION OF THIS PAGE	19. SECURITY CLASSIFICATION OF ABSTRACT	20. LIMITATION OF ABSTRACT
Unclassified	Unclassified	Unclassified	Unlimited

NSN 7540-01-280-5500

Standard Form 298 (Rev. 2-89)
Prescribed by ANSI Std. Z39-18
298-102

NASA-Langley, 1992